NASA TN D-1095

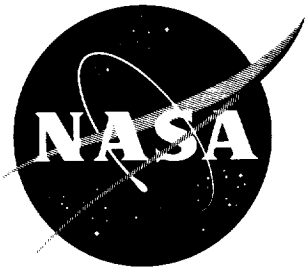

TECHNICAL NOTE

D-1095

INTERACTION OF HIGHLY UNDEREXPANDED JETS

WITH SIMULATED LUNAR SURFACES

By Leonard E. Stitt

Lewis Research Center
Cleveland, Ohio

NATIONAL AERONAUTICS AND SPACE ADMINISTRATION

WASHINGTON December 1961

NATIONAL AERONAUTICS AND SPACE ADMINISTRATION

TECHNICAL NOTE D-1095

INTERACTION OF HIGHLY UNDEREXPANDED JETS WITH SIMULATED LUNAR SURFACES

By Leonard E. Stitt

SUMMARY

Pressure distributions and erosion patterns on simulated lunar surfaces (hard and soft) and interference effects between the surface and two representative lunar vehicles (cylindrical and spherical) were obtained with cold-air jets at various descent heights and nozzle total-pressure ratios up to 288,000.

Surface pressure distributions were dependent on both nozzle area ratio and nozzle contour. Peak pressures obtained with a sonic nozzle agreed closely with those predicted theoretically for a near-sonic jet expanding into a vacuum. Short bell-shaped nozzles gave annular pressure distributions; the low center pressure resulted from the coalescence of shocks that originated within the nozzle. The high surface pressures were contained within a circle whose diameter was about 16 throat diameters, regardless of nozzle area ratio or contour. The peak pressure increased rapidly as the vehicle approached the surface; for example, at a descent height of 40 throat diameters the peak pressure was 0.4 percent of the chamber pressure, but increased to 6 percent at 13 throat diameters.

The exhaust jet eroded a circular concave hole in white sand at descent heights from about 200 to 600 throat diameters. The hole diameter was about 225 throat diameters, while the depth was approximately 60 throat diameters. The sand particles, which formed a conical sheet at a semivertex angle of 50°, appeared to follow a ballistic trajectory and at no time struck the vehicle.

An increase in pressure was measured on the base of the cylindrical lunar vehicle when it approached to within 14 throat diameters of the hard, flat surface. No interference effects were noted between the spherical model and the surface to descent heights as low as 8 throat diameters.

INTRODUCTION

The impingement of hot high-pressure exhaust jets on the lunar surface during "soft" landings or takeoffs may introduce various problems, depending on the constituency of the surface (whether it be soft dustlike or hard rocklike material). For example, the jet impinging on a powdery surface could result in the "digging" of craters, and the presence of possible dust clouds could interfere with the use of navigational and control instrumentation during the landing sequence. The reflection of the hot gases from a hard surface back onto the vehicle might cause both stability and structural problems. At the present time, most of the available information on ground pressure magnitude and distribution is limited to low nozzle pressure ratios.

An experimental cold-flow investigation has been conducted at the Lewis Research Center to determine the pressure distribution and erosion patterns on simulated lunar surfaces, with the exhaust nozzle at various descent heights. Interference effects between a hard flat surface and two representative vehicles were obtained with several nozzle contours and area ratios up to 25 at a total-pressure ratio of 208,000. The erosion pattern caused by the exhaust jet striking a deep layer of white sand was also obtained with area ratios from 1.2 to 500 at a total-pressure ratio of 100,000.

SYMBOLS

A	area, sq in.
d	diameter, in.
l	distance measured along nozzle axis from throat, in.
M	Mach number
P	total pressure, lb/sq in. abs
p	static pressure, lb/sq in. abs
r	radius, in.
x	distance measured along landing surface, in.
y	descent height, in.
α	inclination from vertical, deg
γ	ratio of specific heats

δ angle between jet axis and tangent to jet boundary at nozzle lip, deg

θ_N nozzle exit half-angle, deg

ν Prandtl-Meyer angle, deg

ν_a Prandtl-Meyer angle corresponding to isentropic flow expansion to local ambient pressure

ν_j Prandtl-Meyer angle corresponding to nozzle exit Mach number

Subscripts:

a ambient

b vehicle base

c combustion chamber

j nozzle exit

l condition along nozzle axis

s landing surface

t nozzle throat

v landing vehicle

x condition along x-axis

0 free-stream condition

APPARATUS AND PROCEDURE

The experiments to determine surface and vehicle pressure distributions resulting from the interaction with a highly underexpanded jet were conducted in the 10- by 10-foot supersonic wind tunnel at the Lewis Research Center. When the wind tunnel was operated at a Mach number of 3.5 at a total pressure of 300 pounds per square foot absolute, the measured pressure in the base region of a cone-cylinder-flare body (fig. 1) was about 1 pound per square foot absolute. This body was mounted on a vertical strut, while the simulated lunar vehicles were sting-mounted from a floor strut. The sting could be translated along the tunnel centerline, thus varying the distance between the exhaust nozzle and the simulated lunar surface. Cold air was supplied to the chamber at a pressure

of 2000 pounds per square inch absolute, resulting in a nozzle total-pressure ratio P_c/p_a of 288,000.

Simulated Lunar Surface

The 40-inch-diameter base of the cone-cylinder-flare model (fig. 1) was used as the simulated lunar surface, and the nozzle flow was directed toward this surface. The static-pressure distribution was measured with 17 flush orifices that spanned the flare base. The location of these static-pressure taps with respect to the lunar vehicle can be obtained from the pressure distribution curves. Jet-off static-pressure measurements indicated that the ambient pressure was constant over the model and the base for the range of descent heights investigated.

Lunar Vehicles

The two configurations used as representative lunar vehicles, a 12-inch-diameter by 19.5-inch-long cylinder and a 12-inch-diameter sphere, are shown in figure 2. Descent heights from 0 to 20 inches were obtained when these vehicles were translated by the sting. The majority of the data was obtained with a single nozzle (fig. 2(a)). One configuration, however, was investigated with a cluster of four nozzles (fig. 2(b)) designed for a total airflow equal to that of the single nozzle. Both of the lunar vehicles were instrumented with 20 flush orifices to determine changes in external static-pressure distributions.

Approach Conditions

The lunar vehicle is shown in figure 3(a) in a vertical landing or takeoff attitude with respect to the simulated lunar surface. The effects of a surface discontinuity were obtained with a 2- by 5- by 10-inch block, shown in figure 3(b). The centerline of the jet intercepted the long side of the block at its midpoint. Three static-pressure taps were located on top of the block in a line with the base plate instrumentation. One configuration was investigated with the vehicle axis inclined at 5° with respect to a line perpendicular to the surface, and is shown in this attitude in figure 3(c).

Exhaust Nozzles

The effects of varying nozzle area ratio were obtained with a sonic nozzle and three 15°-half-angle conical nozzles having area ratios A_j/A_t of 4, 15, and 25 (fig. 4(a)). Each of the single-nozzle configurations had a throat diameter of 0.50 inch and a total flow of about 10

pounds of air per second at a chamber pressure of 2000 pounds per square inch absolute. All four of the contoured nozzles (figs. 4(b) to (e)) had area ratios of 25, resulting in exit diameters of 2.50 inches.

A short overturned bell nozzle (fig. 4(b)) with the length arbitrarily fixed at 80 percent of an equivalent 15° conical nozzle was investigated. The contour was formed by a conic section tangent to the throat arc and exit angle. The four nozzles of the clustered configuration were scaled versions of this nozzle having a total weight flow equal to that of the single nozzle. Each of these smaller nozzles thus had a throat diameter of 0.25 inch and an exit diameter of 1.25 inches. Preliminary results obtained with this nozzle indicated that the overturning of the flow resulted in internal disturbances within the expanding jet that greatly influenced the surface pressure distributions. Three additional nozzles of varying length and exit angle were therefore investigated to determine the effects of nozzle contour. The short isentropic nozzle (fig. 4(c)) also had a length 80 percent of an equivalent 15° conical nozzle. The design of this nozzle contour, a parabola tangent to the throat radius and exit angle, was based on results presented in reference 1. The truncated isentropic nozzle contour was obtained from reference 2 (designated as a cutoff isentropic nozzle in this report), and the long isentropic nozzle shape was obtained from reference 3. Coordinates for all the contoured nozzles are listed in table I. Each of the nozzles was instrumented with one internal static-pressure orifice at the exit plane and two external static-pressure taps.

Determination of Surface Erosion

In addition to the tests conducted in the wind tunnel, qualitative investigations were carried out in a 4- by 6-foot vacuum facility (fig. 5) to explore visually the erosion caused by the impingement of an underexpanded jet on a thick layer of 0.010-inch-diameter, white-sand particles. Cold air at a pressure of 150 pounds per square inch absolute was supplied to a small nozzle having a throat diameter of 1/32 inch and a corresponding weight flow of 0.00224 pound per second. A conical nozzle with an area ratio of 12 and contoured nozzles with area ratios of 150 and 500 were tested at descent heights ranging from about 200 to 600 throat diameters. The experimental runs lasted for 2.7 seconds, during which time the vacuum tank pressure increased from an initial value of 8×10^{-2} millimeter to 8×10^{-1} millimeter of mercury. Nozzle total-pressure ratio thus dropped from 100,000 to 10,000 during this cycle. Erosion patterns were recorded photographically through a glass window on one end of the tank (fig. 5).

RESULTS AND DISCUSSION

Surface Pressure Distribution

The schlieren photographs (fig. 6, e.g.) are arranged to show the lunar vehicle in a vertical landing or takeoff attitude and are presented to the same scale as the abscissa of the pressure distribution curves. The centerline of the nozzle is alined with the $x = 0$ point on the surface. All the measured pressures were put in nondimensional form by dividing by the chamber pressure. Two indications of descent heights, y_j/d_t and y_t/d_t, are given on the figures for each position of the model and are the distances measured from the lunar surface to the nozzle exit plane and the nozzle throat, respectively. In the following discussion, the descent height referred to will be the distance from the surface to the nozzle throat.

Effect of nozzle area ratio. - The initial expansion angle δ between the jet axis and a tangent to the jet boundary at the nozzle lip is indicative of the amount of jet spreading. As would be expected, this angle decreased with increasing nozzle area ratio, as shown in the schlieren photographs of figure 6. For this range of area ratios (1 to 25), the nozzle total-pressure ratio P_c/p_a remained constant at a value of 288,000. However, the nozzle static-pressure ratio p_j/p_a, which is an index of jet spreading, varied from 152,000 for the sonic exit to 545 for the nozzle with an area ratio of 25 and a corresponding exit Mach number of 5.0.

At the largest descent height (approx. 40 throat diam) the surface pressures were low and, in general, uniformly distributed with the sonic nozzle (fig. 6(a)). As the nozzle area ratio increased, at the same distance, the surface pressure also increased; however, with an area ratio of 25, the maximum pressure was only about 0.3 percent of the chamber pressure (fig. 6(d)). The shape of the pressure curves with decreasing values of descent height was generally symmetrical with the peak value on the jet centerline. A maximum surface pressure of 5 percent of chamber pressure was recorded for the 25-to-1 conical nozzle at a descent height of 10 throat diameters. In general, the high pressures were contained within a circle whose diameter was equal to about 16 throat diameters, regardless of nozzle area ratio.

In reference 4, the method of characteristics was used to compute a Mach number distribution along the axis of symmetry for a cold jet of air ($\gamma = 1.4$) issuing from a near-sonic orifice into a vacuum. This theoretical Mach number distribution, shown as a dashed line in figure 7(a), was used to compute a theoretical peak surface pressure as a function of distance from the nozzle throat. As seen in the schlieren photographs of figure 6, a normal shock stands slightly off the landing

surface. The ratio of surface pressure, measured on the jet centerline, to chamber pressure should be approximately equal to the normal shock recovery associated with the centerline Mach number. This, in turn, is a function of the distance from the nozzle throat, or descent height. The peak surface pressures measured for the sonic nozzle (fig. 7(b)) compare favorably with the theoretical curve. This is perhaps significant in assessing the quality of lunar simulation achieved, in that the theory assumed an infinite pressure ratio while the measured data were obtained at a finite pressure ratio of 288,000. Condensation of both nitrogen and oxygen may be anticipated at this high pressure ratio; however, both the schlieren observations and the pressure measurements indicate that, if condensation did occur, the effects were small.

As the area ratio is increased, the physical divergent portion of the nozzle does not allow the jet to expand as rapidly as it would from a sonic nozzle in the same distance. The solid symbols in figure 7(a) indicate the theoretical nozzle exit Mach number M_j. The normal shock recovery based on that Mach number for each nozzle is plotted in figure 7(b), also as solid symbols.

The measured centerline Mach numbers and corresponding surface pressures for the conical nozzles are also presented in figure 7. At a distance of 40 throat diameters, the lowest Mach number on the centerline was about 10 for the 25-to-1 nozzle. Mach numbers off the centerline, at the same distance from the throat, are, of course, higher.

Effect of nozzle contour. - The schlieren photographs of figure 8 indicate that all the contoured nozzles had some type of shock structure within the jet that extended several throat diameters downstream. These internal disturbances were not as apparent with the conical nozzles. The strength of the shocks appeared to be a function of the rate of turning and, as expected, was more pronounced for the two short configurations (figs. 8(a) and (b)). The largest effect was shown with the short overturned bell nozzle having an exit half-angle of 3.4° (fig. 8(a)). From the schlieren photographs it appeared that the shocks, which originated inside the nozzle, coalesced into a normal shock on the nozzle centerline downstream of the exit. The low-energy core associated with this coalescence persisted farther downstream and resulted in the annular pressure distribution measured on the surface. Although the internal disturbances altered the shape of the pressure-ratio curves, as compared with those obtained with the conical nozzles, the high pressures again were contained within a circle whose diameter was about 16 nozzle throat diameters.

The peak surface pressures were also affected by the internal shock systems, especially in the region immediately downstream of the nozzle exit, as can be seen by the increase in peak pressure with distance in figure 9. The tailed symbols show points where the peak surface pressure

was measured off of the nozzle centerline and indicate, therefore, an annular surface pressure distribution. At a distance of 40 throat diameters, the peak surface pressures again were very low, and of the same order of magnitude as that obtained with the equivalent conical nozzle. The largest surface pressures obtained with the contoured nozzles was about 0.06 times the chamber pressure at a descent height of 13 throat diameters and 0.004 times at a descent height of 40.

Effect of clustering nozzles. - The use of four jets with a total weight flow equivalent to a single nozzle appeared to be effective in eliminating a large part of the annular pressure distribution that was obtained with the single nozzle. However, each of the four nozzles had the same type of shock pattern emanating from its exit as did the single nozzle (fig. 10 compared with fig. 8(a)). The clustered configuration, in general, had lower peak surface pressures than the single nozzle, as shown in figure 13. The region of high pressure again was contained within a circle whose diameter was 16 throat diameters, probably because of the very close spacing of the nozzles.

Effect of a surface discontinuity. - A surface discontinuity, in the form of a rectangular block (fig. 11), had a surface pressure distribution very different from that obtained for a flat surface. The block appeared to redistribute the flow over a larger surface area; and, as a result, the peak pressure was considerably less than that obtained without the discontinuity (fig. 13).

Effect of operation at 5° inclination from vertical. - Operation of the landing vehicle at 5° inclination from vertical (fig. 12) resulted in a slightly asymmetrical surface pressure distribution, with peak pressures occurring slightly to one side of the centerline. The annular pressure distribution obtained at 0° inclination is not apparent, although there may not have been sufficient surface instrumentation to pick up the low-energy core, which is evident in the schlieren photograph. The peak surface pressures again were lower than those obtained at 0° inclination (fig. 13).

Reflection Effects on Lunar Vehicles

There was no detectable change in the surface pressure distribution on the spherical configuration even when the distance between the lunar surface and the surface of the sphere was only 8 throat diameters. At comparable positions, a pressure increase was measured on the cylindrical vehicle, but only on the surface parallel to the landing surface. The pressure increase, which, in general, occurred initially at about a descent height of 14 throat diameters for the 25-to-1 nozzles, is shown in figure 14.

The shock patterns obtained near the base of the cylinder at close proximity to the lunar surface are shown in the schlieren photographs of figure 15. The flow appeared to be contained somewhat between the two parallel surfaces; as mentioned previously, this was not the case with the spherical model. A symmetrical shock pattern was obtained in all cases except with a surface discontinuity and operation at 5° inclination from vertical, as would be anticipated. The asymmetrical flow is evident in the schlieren photographs of figures 15(c) and (d). The asymmetry gives rise to a vehicle moment, which is destabilizing for a surface discontinuity and stabilizing for operation at 5° inclination.

Comparison of Theoretical and Experimental Jet Expansion Boundaries

There are several methods available (e.g., refs. 5 to 7) to compute the initial contour of a supersonic jet exhausting into quiescent air. All of these methods depend on an accurate prediction of nozzle exit flow conditions (M_j and γ_j) and initial inclination angle δ. The flow conditions at the nozzle exit were based on one-dimensional flow considerations within the nozzle. The initial inclination angle was computed by assuming that the flow expands isentropically to ambient pressure. In equation form,

$$\delta = \nu_a - \nu_j + \theta_N$$

The circular-arc approximation (ref. 7), which is empirical in nature, underestimated the jet boundary to some extent (fig. 16). It was observed, however, that the initial inclination angle was always from 6° to 9° higher than that predicted by Prandtl-Meyer expansion assuming one-dimensional flow. When the theory was adjusted to the measured inclination angle, it gave a reasonable estimate of the jet boundary, as shown.

Surface Erosion Patterns Obtained in a Thick Layer of Sand

In the 4- by 6-foot vacuum facility, the tank pressure increased during nozzle operation at the rate of 0.280 millimeter per second with the addition of 0.00224 pound of air per second. The running time for each of the test points was therefore limited to about 2.7 seconds, and during this time the nozzle total-pressure ratio decreased from 100,000 to 10,000. The following qualitative observations were made and should be considered in the light of these limitations.

During the initial start of the flow from the nozzle a curious erosion pattern was obtained, as shown in figure 17. The jet eroded an annular depression in the sand, while the central area remained intact. Surface erosion patterns of this type were also observed from the downwash of VTOL aircraft, as reported in reference 8. The erosion progressed toward the center with time; a central peak formed and projected briefly above the surface and then collapsed. This phenomenon, which generally occurred during the first 0.5 second, was more pronounced at the lower descent heights where the interior peak was higher and lasted longer. The jet continued to "dig" a large circular concave hole, such as that shown in figure 18, after the elimination of the central peak.

The final hole depth and diameter were recorded photographically, and the following general results were obtained:

(1) Variations in nozzle area ratio from 12 to 500 had little measurable effect on either the depth or diameter of the hole.

(2) As descent height decreased from 575 to 192 throat diameters, the hole diameter increased from 200 to 250 throat diameters while the depth remained essentially constant at about 30 throat diameters.

(3) The sand particles were thrown upward and outward in a sheet forming essentially a conical surface with a semivertex angle that averaged about 50°. However, since the particles apparently followed a ballistic trajectory, at no time did any of the sand strike the vehicle. Maximum particle heights were estimated to be about 480 throat diameters.

It should be pointed out that an infinite dust layer was assumed in these experiments while the actual constituency of the lunar surface may be considerably different. Under conditions of a very high vacuum (10^{-6} to 10^{-9} mm Hg), grain packing and adhesion properties may become important so that a hard surface may be the more realistic lunar model.

SUMMARY OF RESULTS

An experimental program has been conducted to study the interaction effects of a highly underexpanded jet impinging on simulated hard and soft lunar surfaces. The results were obtained with cold-air jets at nozzle pressure ratios up to 288,000. Although exploratory in nature, the study indicates trends and first-order effects pertinent to the gas dynamics associated with a rocket-powered vehicle operating in close proximity to a "lunar" surface, such as in "soft" landings or during the launch period. Variations in nozzle geometry and surface constituency are included.

Detailed results and observations are as follows:

1. Pressure distribution on a hard flat surface

(a) Surface pressure distributions were dependent on nozzle area ratio. The peak pressure obtained with a sonic nozzle at descent heights from 2 to 40 throat diameters agreed closely with those predicted theoretically for a near-sonic jet expanding into a vacuum.

(b) Surface pressure distributions were also dependent on nozzle contour. For example, the short bell-shaped nozzles gave annular surface pressure distributions, which resulted from the coalescence of shocks originating within the nozzle.

(c) The high pressure area was small in diameter compared with the diameter of the billowing jet. In general, the high pressures were contained within a circle whose diameter was about 16 throat diameters, regardless of area ratio or nozzle contour.

(d) The surface pressures increased rapidly as the vehicle approached the simulated lunar surface. For example, the maximum pressure at a descent height of 40 throat diameters was only 0.4 percent of the chamber pressure, but increased to 6 percent at 13 throat diameters.

2. Surface erosion in sand

(a) At descent heights from about 200 to 600 throat diameters, a circular hole was "dug" in white sand used to simulate a soft lunar surface. The diameter of the hole was about 225 throat diameters, while the depth was approximately 60 throat diameters.

(b) Sand particles, thrown upward, formed a cone with a semivertex angle of about 50°. The particles, apparently following a ballistic trajectory, at no time struck the vehicle.

3. Interactions between the surface and lunar vehicles

(a) An increase in pressure was measured on the base of the cylindrical configuration when it approached to within 14 throat diameters of the hard, flat surface.

(b) A spherical model appeared to be effective in eliminating the interference effects, at least to descent altitudes as low as 8 throat diameters.

(c) Both a surface discontinuity and operation at 5° inclination from vertical resulted in asymmetrical pressure distributions on the base of the cylindrical model when in close proximity to the surface.

Lewis Research Center
National Aeronautics and Space Administration
Cleveland, Ohio, August 17, 1961

REFERENCES

1. Rao, G. V. R.: Approximation of Optimum Thrust Nozzle Contour. ARS Jour., vol. 30, no. 6, June 1960, pp. 561-563.

2. Sivo, Joseph N., Meyer, Carl L., and Peters, Daniel J.: Experimental Evaluation of Rocket Exhaust Diffusers for Altitude Simulation. NASA TN D-298, 1960.

3. Rao, G. V. R.: Contoured Rocket Nozzles. Paper presented at Ninth Annual Cong. Int. Astronautical Federation (Amsterdam), Aug. 25-30, 1958.

4. Owen, P. L., and Thornhill, C. K.: The Flow in an Axially-Symmetric Supersonic Jet from a Nearly-Sonic Orifice into a Vacuum. R.&M. 2616, British ARC, Sept. 1962.

5. Love, Eugene S., Grigsby, Carl E., Lee, Louise P., and Woodling, Mildred J.: Experimental and Theoretical Studies of Axisymmetric Free Jets. NASA TR R-6, 1959.

6. Englert, Gerald W.: Operational Method of Determining Initial Contour of and Pressure Field About a Supersonic Jet. NASA TN D-279, 1960.

7. Latvala, E. K.: Spreading of Rocket Exhaust Jets at High Altitudes. TR-59-11, Arnold Eng. Dev. Center, June 1959.

8. Kuhn Richard E.: An Investigation to Determine Conditions Under Which Downwash from VTOL Aircraft Will Start Surface Erosion from Various Types of Terrain. NASA TN D-56, 1959.

TABLE I. - COORDINATES FOR CONTOURED EXIT NOZZLES

Short isentropic, $\theta_N = 10.1^\circ$		Short overturned bell, $\theta_N = 3.4^\circ$		Truncated isentropic, $\theta_N = 9.9^\circ$		Long isentropic, $\theta_N = 2.2^\circ$	
l/d_t	d_l/d_t	l/d_t	d_l/d_t	l/d_t	d_l/d_t	l/d_t	d_l/d_t
0	1.00	0	1.00	0	1.00	0	1.00
.10	1.05	.27	1.15	.14	1.01	.17	1.02
.22	1.19	.50	1.42	.27	1.07	.37	1.15
.37	1.35	1.00	1.98	.40	1.17	.53	1.27
.52	1.53	1.50	2.51	.54	1.29	.74	1.44
.68	1.70	2.00	3.00	.67	1.41	1.06	1.69
.84	1.87	2.50	3.44	1.00	1.69	1.37	1.93
1.09	2.12	3.00	3.84	1.34	1.97	1.69	2.16
1.21	2.22	3.50	4.17	1.67	2.22	1.89	2.30
1.33	2.34	4.00	4.46	2.00	2.49	2.11	2.44
1.59	2.57	4.50	4.67	2.34	2.73	2.43	2.63
1.91	2.83	5.00	4.84	2.67	2.95	2.74	2.81
2.12	3.00	5.50	4.94	3.00	3.16	3.05	2.98
2.38	3.19	6.00	5.00	3.34	3.35	3.37	3.13
2.63	3.37			3.67	3.54	3.69	3.28
2.90	3.54			4.00	3.72	4.01	3.42
3.18	3.71			4.34	3.88	4.32	3.54
3.47	3.88			4.67	4.04	4.85	3.73
3.79	4.05			5.00	4.20	5.37	3.91
4.12	4.22			5.34	4.34	5.80	4.04
4.48	4.40			5.67	4.48	6.31	4.18
4.86	4.56			6.00	4.60	6.84	4.32
5.28	4.73			6.34	4.73	7.37	4.44
5.73	4.90			6.67	4.85	7.90	4.55
6.00	5.00			7.10	5.00	8.53	4.66
						9.05	4.74
						9.70	4.84
						10.23	4.90
						10.73	4.96
						11.25	5.00

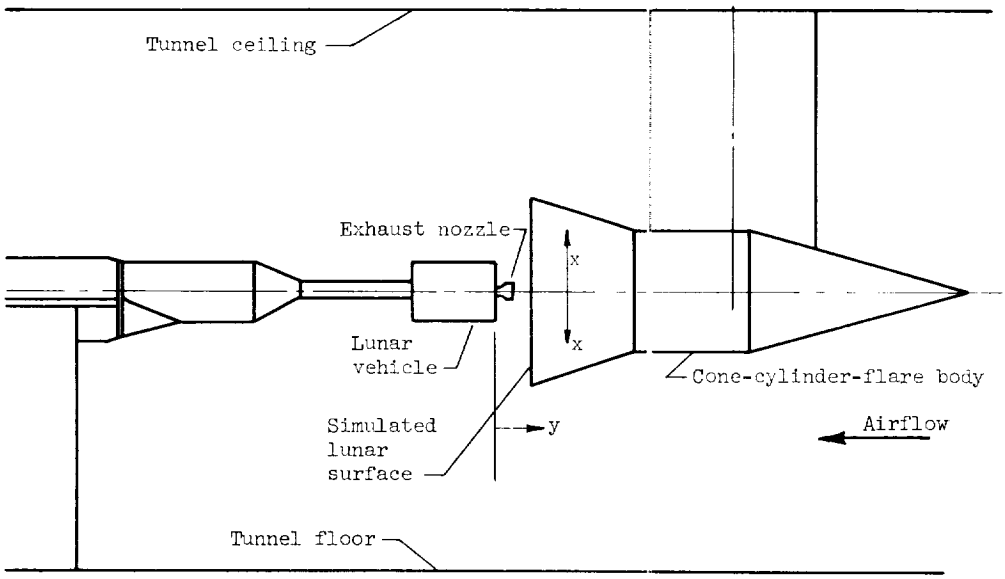

Figure 1. - Installation of model in 10- by 10-foot supersonic wind tunnel. M_O, 3.5; P_O, 300 pounds per square foot absolute.

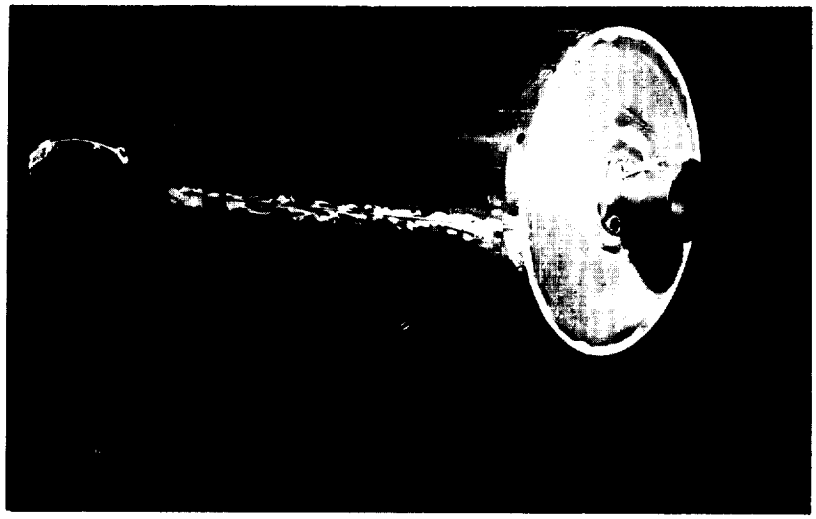

(a) Cylinder with 25:1 area ratio nozzle. (Cylinder, 12-in. diam. by 19.5-in. length.)

(b) Sphere with cluster of four 25:1 area ratio nozzles. (Sphere, 12-in. diam.)

Figure 2. - Experimental configurations.

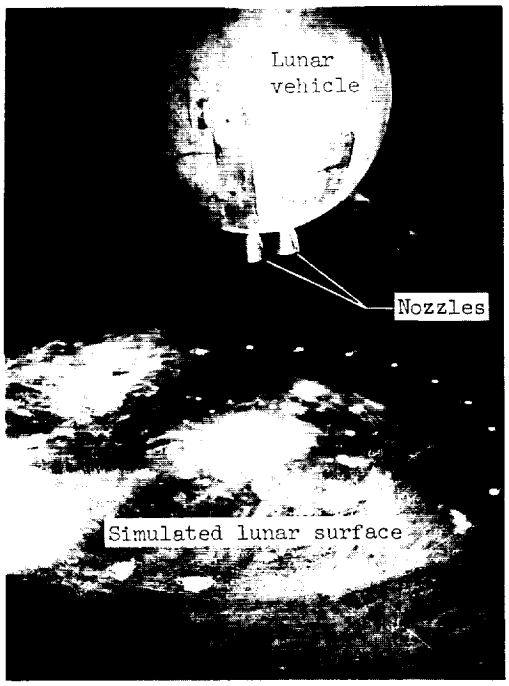

(a) Sphere approaching flat surface.

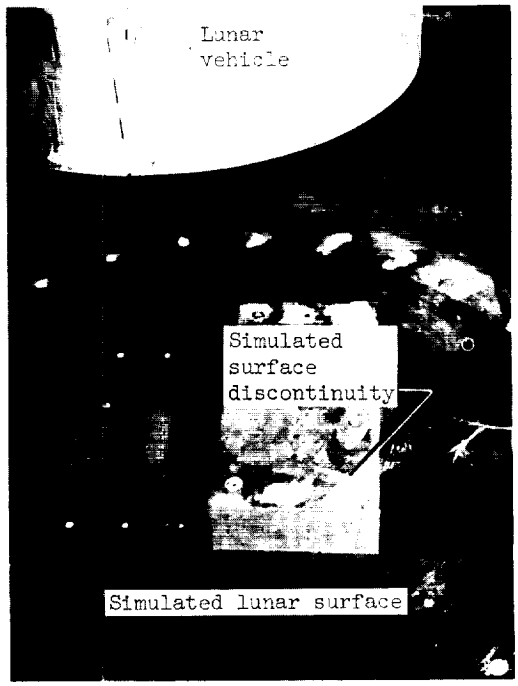

(b) Cylinder approaching surface discontinuity.

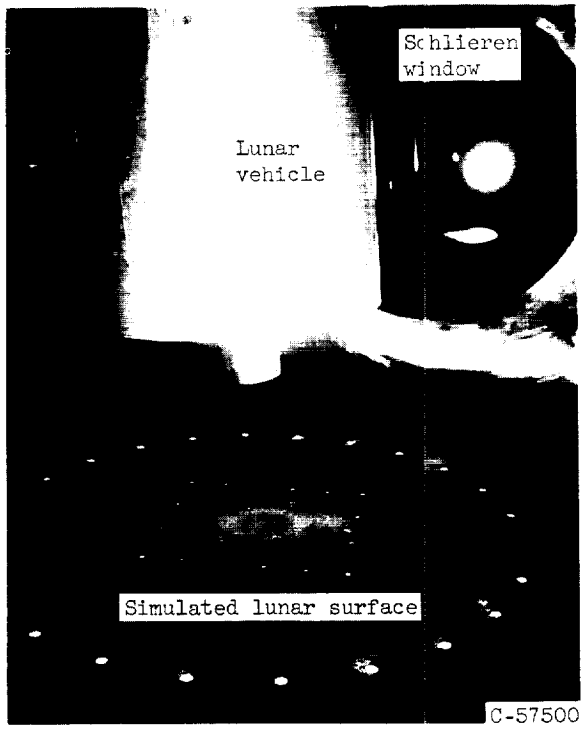

(c) Cylinder approaching flat surface at 5° inclination from vertical.

Figure 3. - Approach conditions.

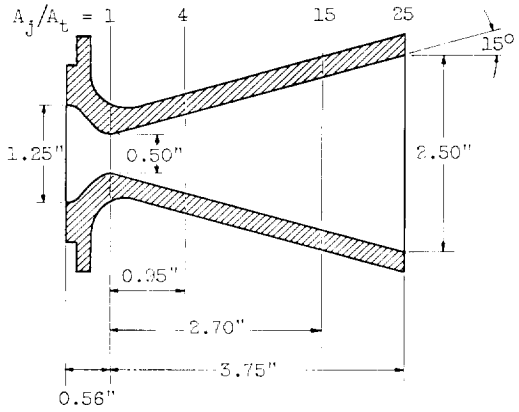

(a) Sonic and conical nozzles.

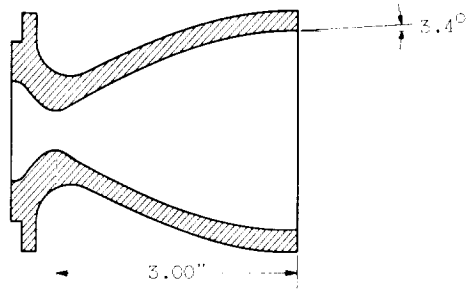

(b) Short overturned bell nozzle.

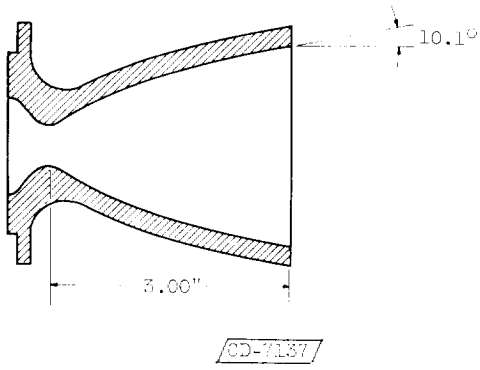

(c) Short isentropic nozzle.

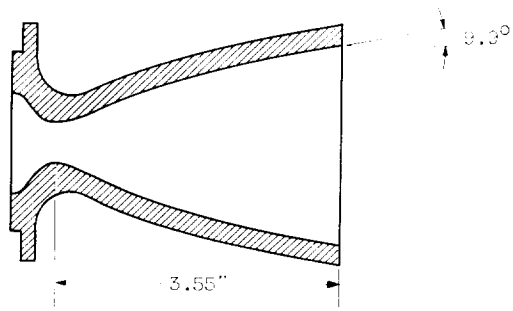

(d) Truncated isentropic nozzle.

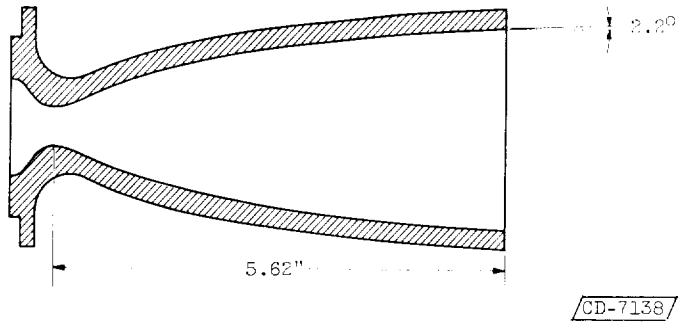

(e) Long isentropic nozzle.

Figure 4. - Nozzle details.

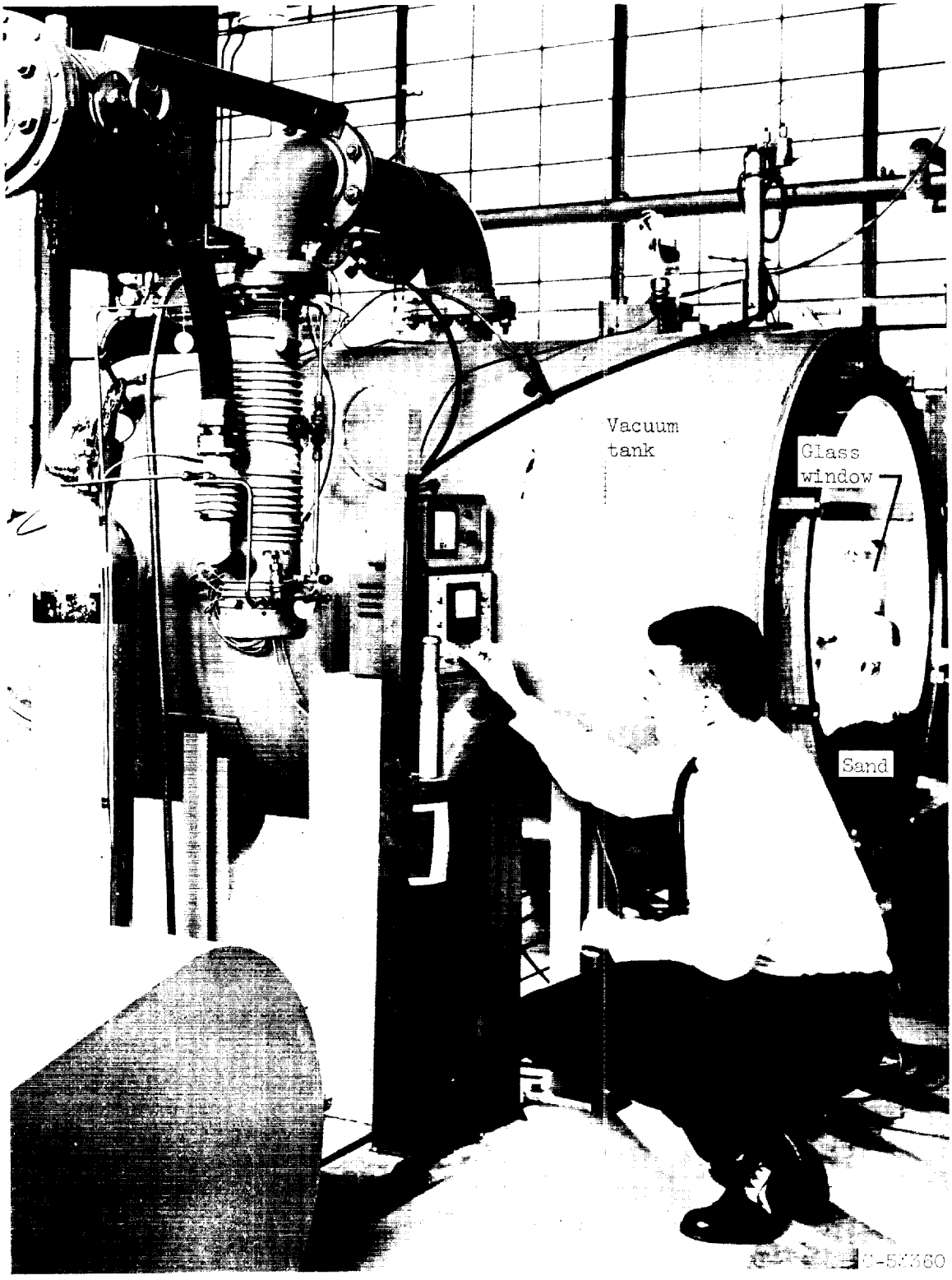

Figure 5. - 4- by 6-foot vacuum facility.

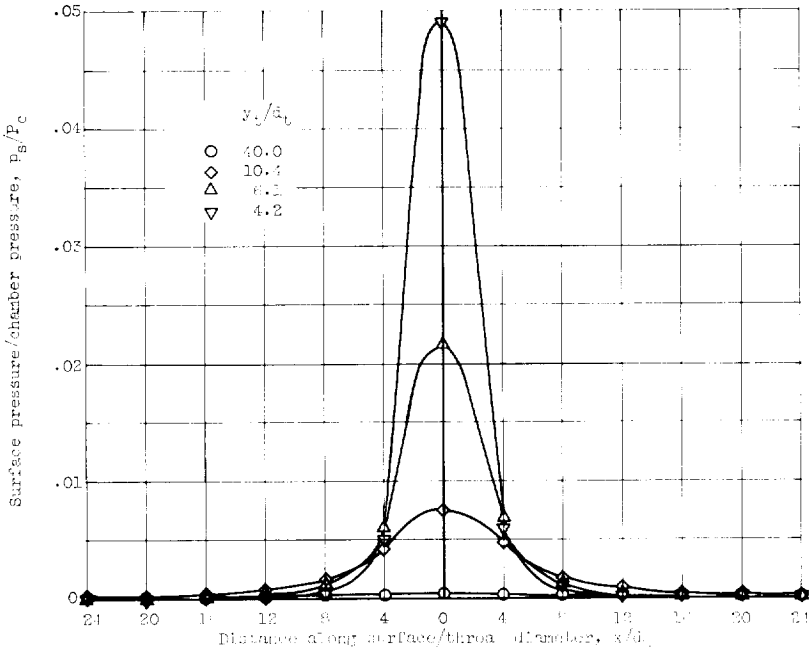

(a) Sonic nozzle. $A_j/A_t = 1.0$; $\varepsilon_N = 0°$; $z/d_t = 0$; $p_1/p_a = 100,000$.

Figure 7. - Effect of nozzle area ratio on lunar surface pressure distribution.

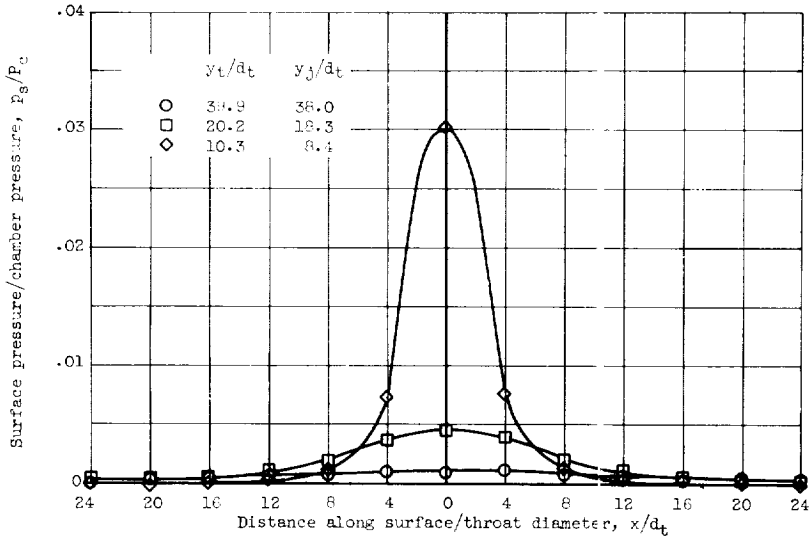

(b) Conical nozzle. $A_j/A_t = 4.0$; $\theta_N = 15°$; $l/d_t = 1.9$; $p_j/p_a = 8600$.

Figure 6. - Continued. Effect of nozzle area ratio on landing surface pressure distribution.

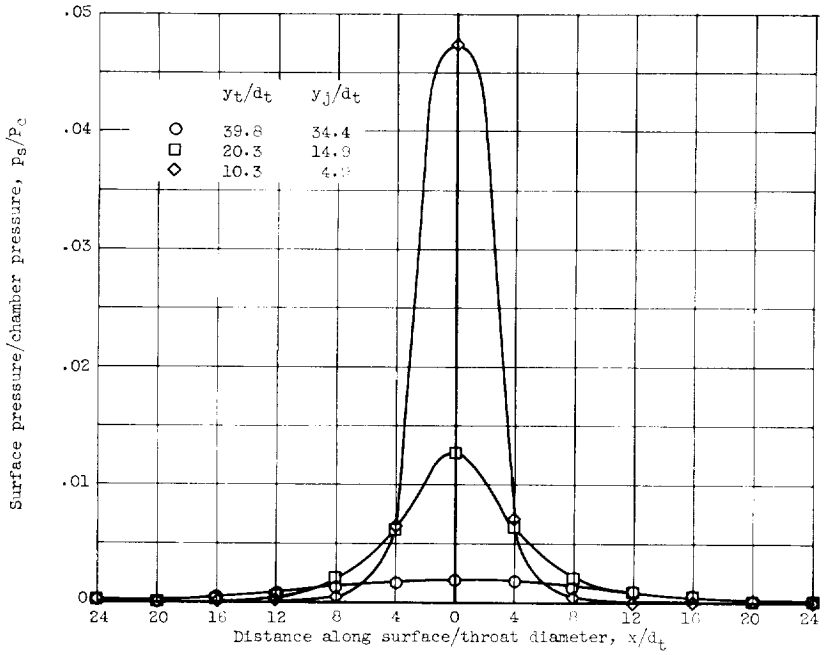

(c) Conical nozzle. $A_j/A_t = 15.0$; $\theta_N = 15°$; $l/d_t = 5.4$; $p_j/p_a = 1152$.

Figure 6. - Continued. Effect of nozzle area ratio on landing surface pressure distribution.

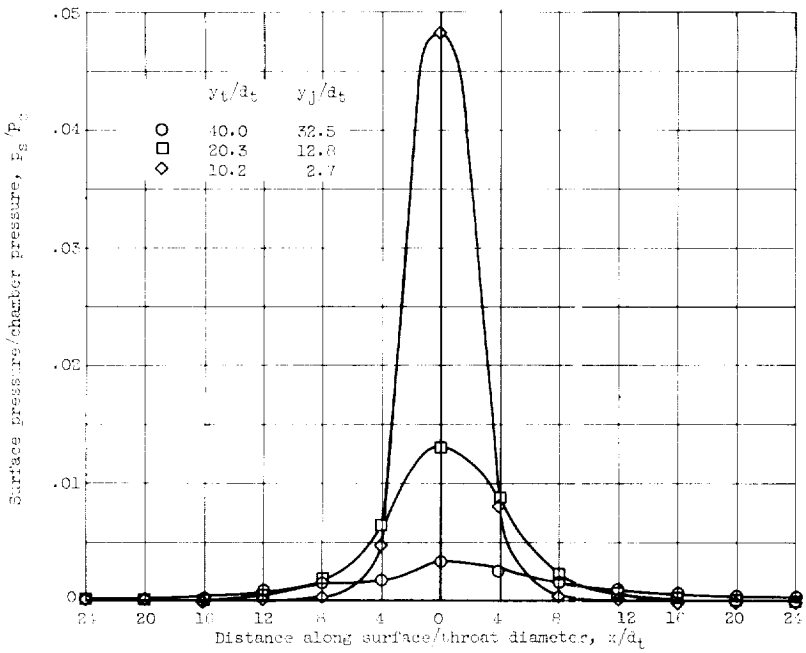

(i) Conical nozzle. A_j/A_t = 29.0; θ_N = 15°; l/d_t = 7.5; P_j/P_a = 545.

Figure 7. - Concluded. Effect of nozzle area ratio on landing surface pressure distribution.

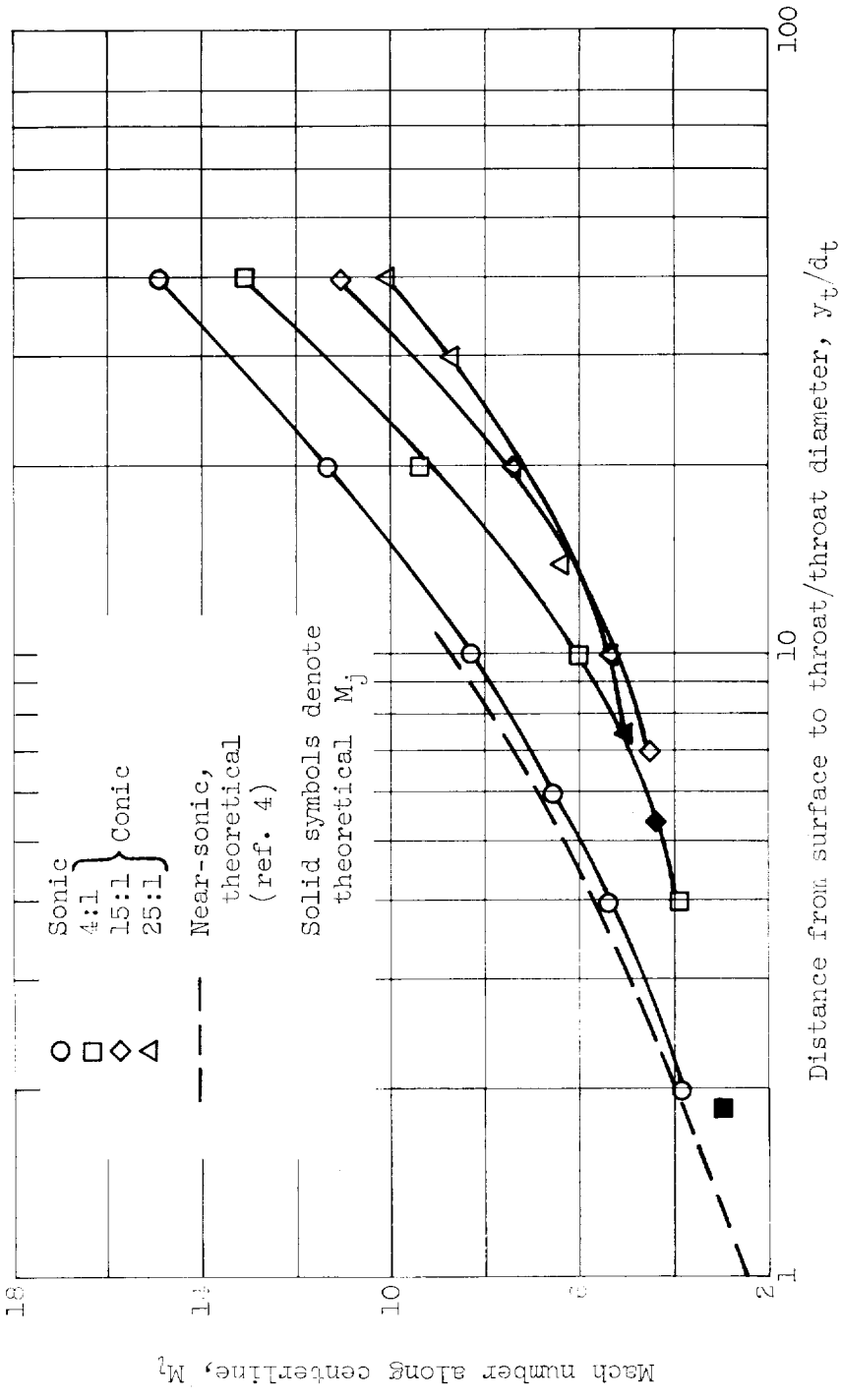

(a) Mach number corresponding to peak pressure.

Figure 7. - Effect of nozzle area ratio on peak surface pressure and corresponding flow Mach number.

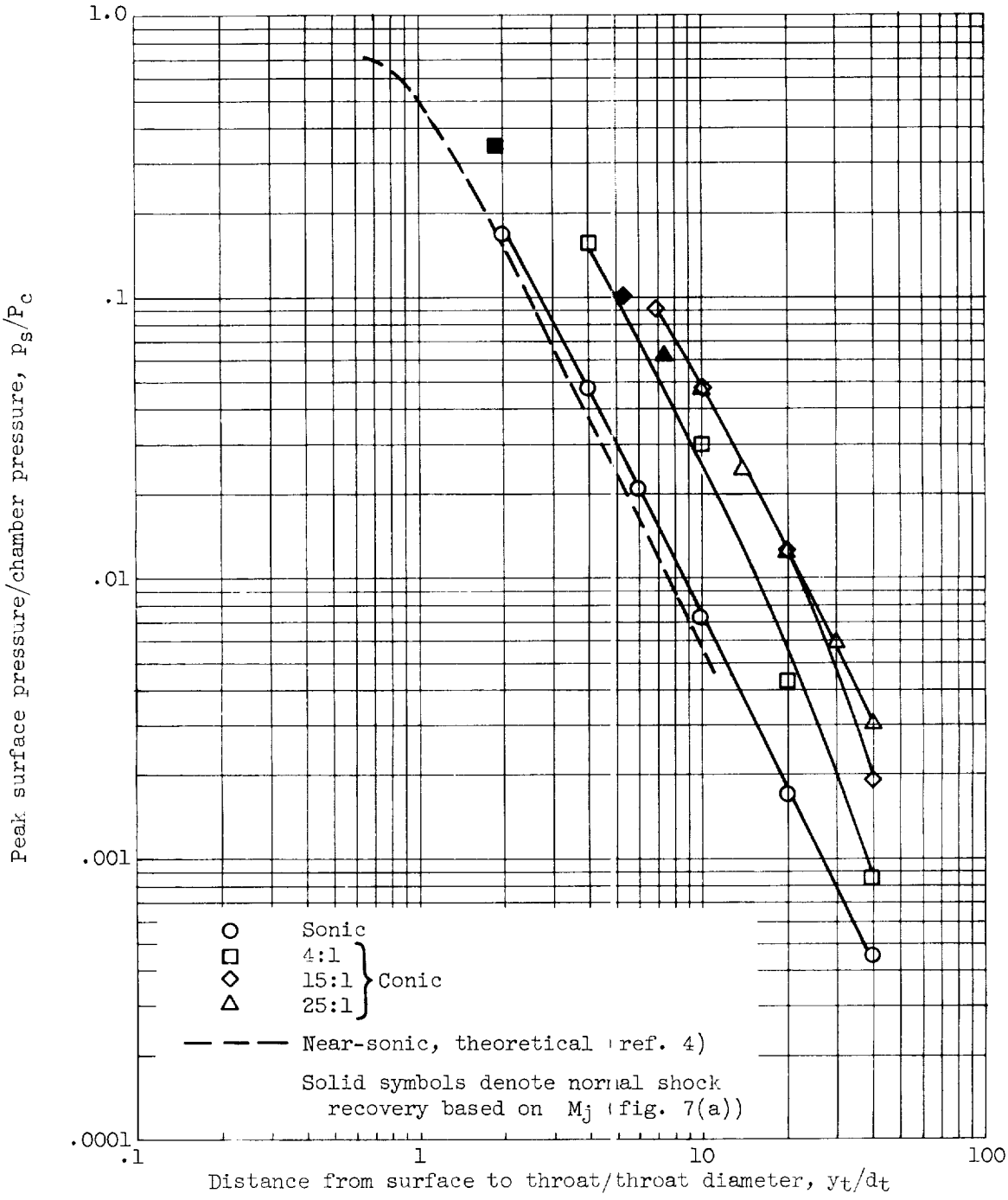

(b) Peak surface pressure.

Figure 7. - Concluded. Effect of nozzle area ratio on peak surface pressure and corresponding flow Mach number.

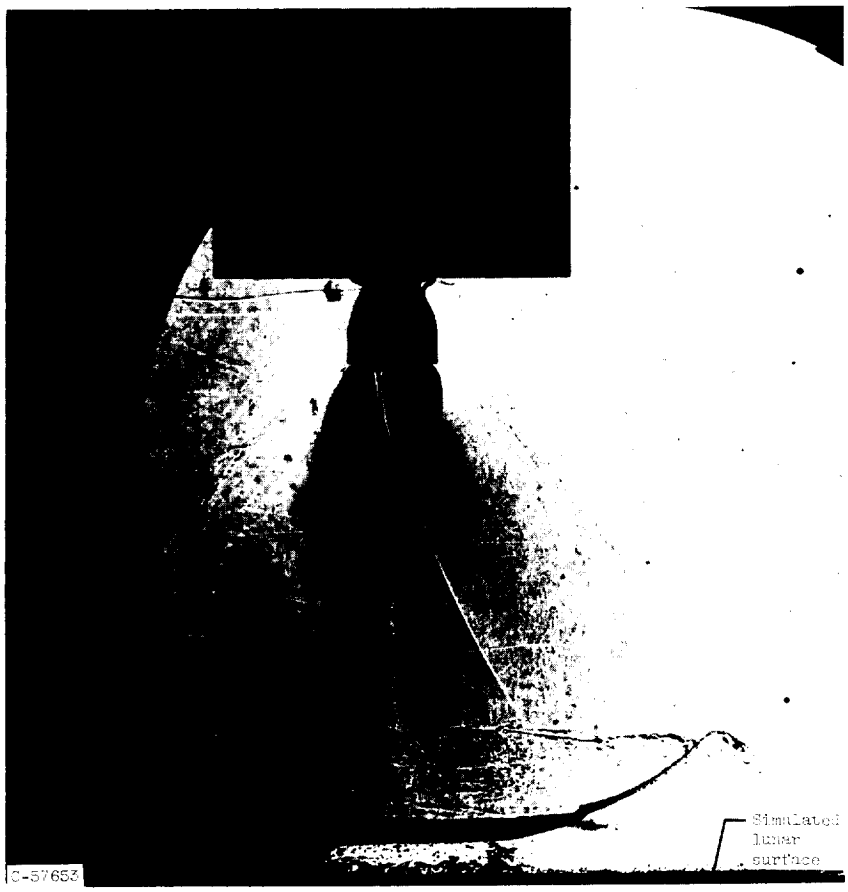

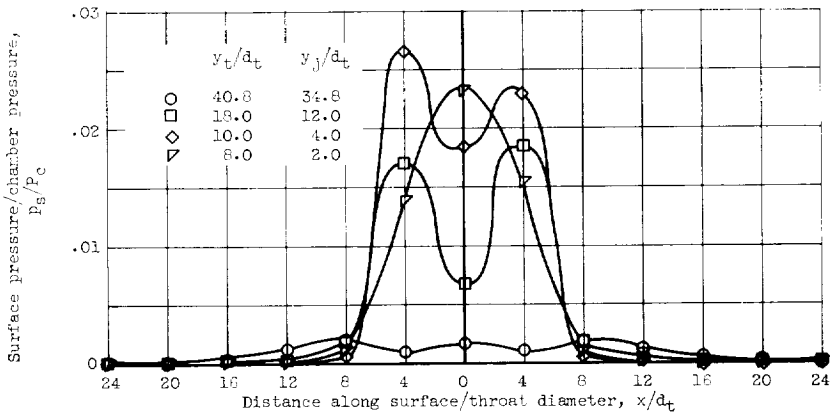

(a) Short overturned bell nozzle. $\theta_N = 3.4^\circ$; $l/d_t = 6.0$.

Figure 8. - Effect of nozzle contour on landing surface pressure distribution. $A_j/A_t = 25$; $p_j/p_a = 545$.

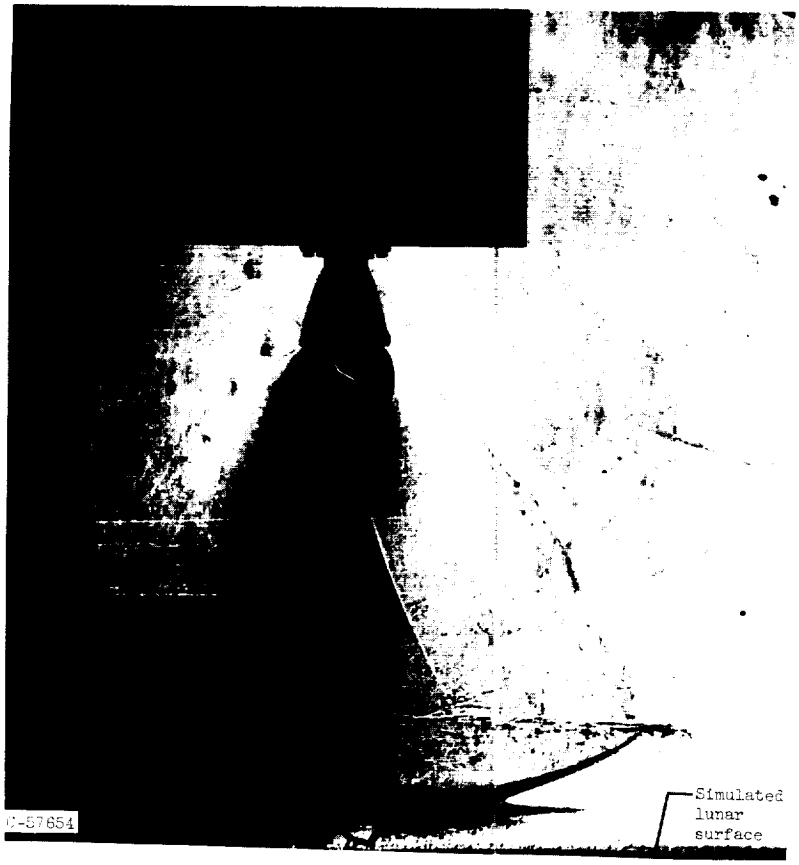

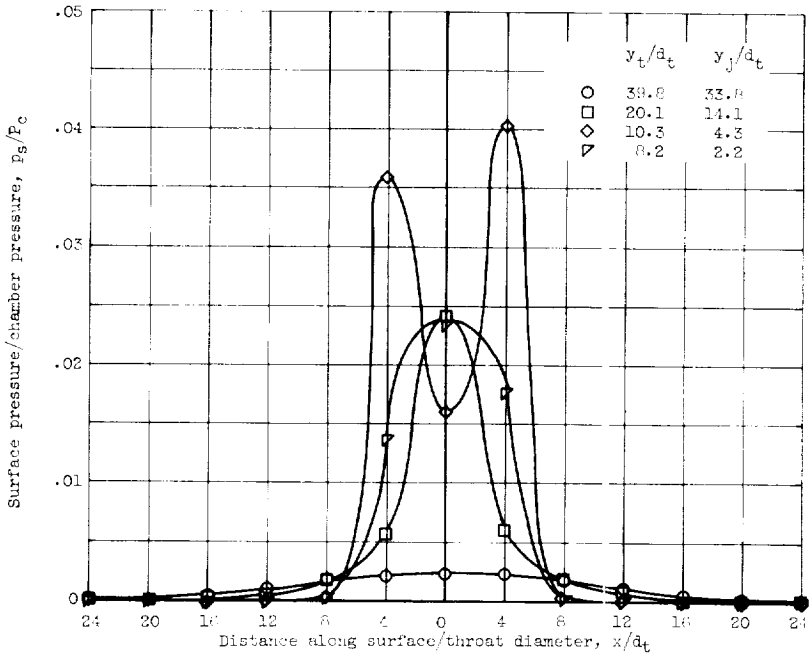

(b) Short isentropic nozzle. $\theta_N = 10.1°$; $l'/d_t = 0.0$.

Figure 8. - Continued. Effect of nozzle contour on landing surface pressure distribution. $A_j/A_t = 25$; $p_j/p_a = 545$.

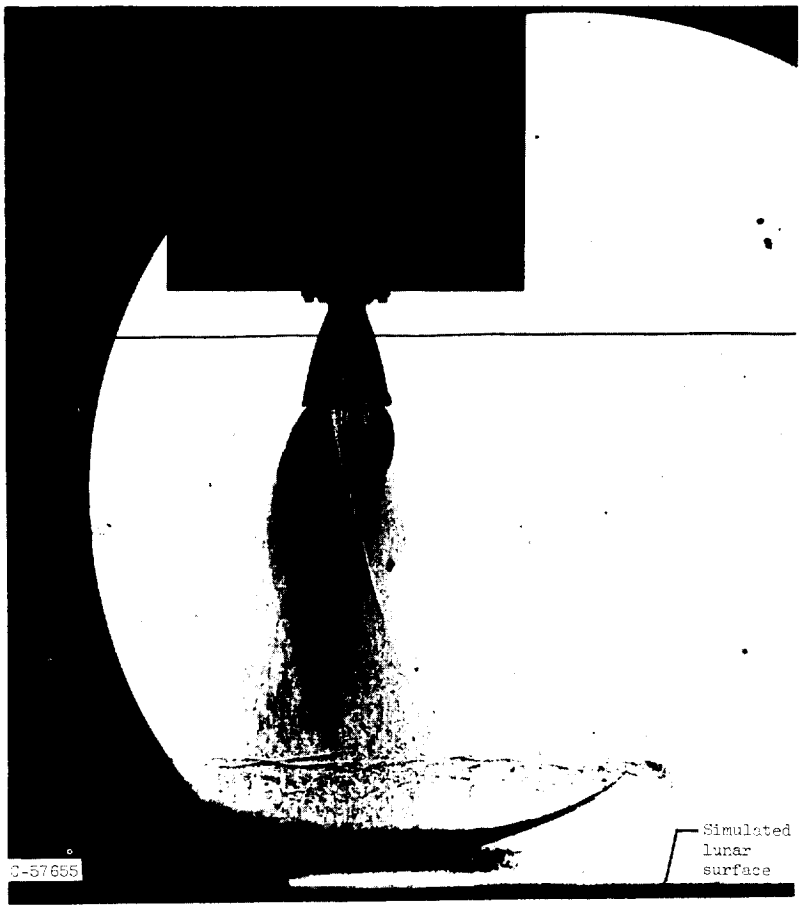

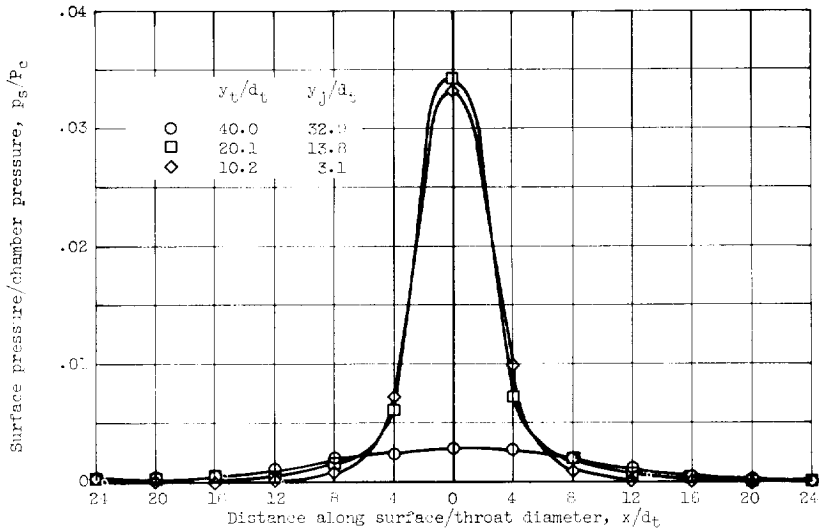

(c) Truncated isentropic nozzle. θ_N = 3.4°; l/d_t = 7.1.

Figure 8. - Continued. Effect of nozzle contour on landing surface pressure distribution. A_j/A_t = 25; p_j/p_a = 545.

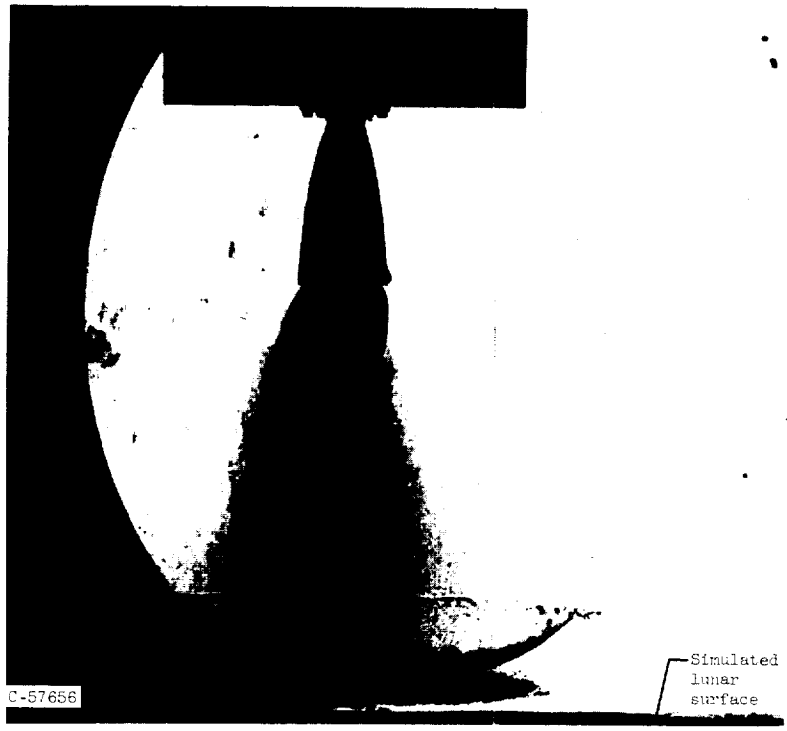

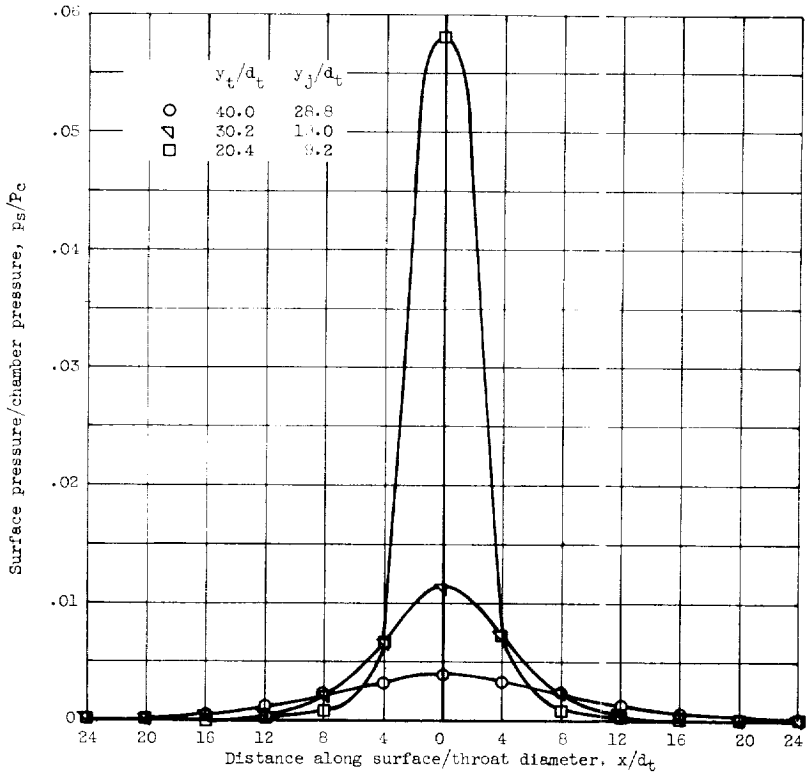

(d) Long isentropic nozzle. $\theta_N = 2.2°$; $l/a_t = 11.24$.

Figure 8. - Concluded. Effect of nozzle contour on landing surface pressure distribution. $A_j/A_t = 25$; $p_j/p_a = 545$.

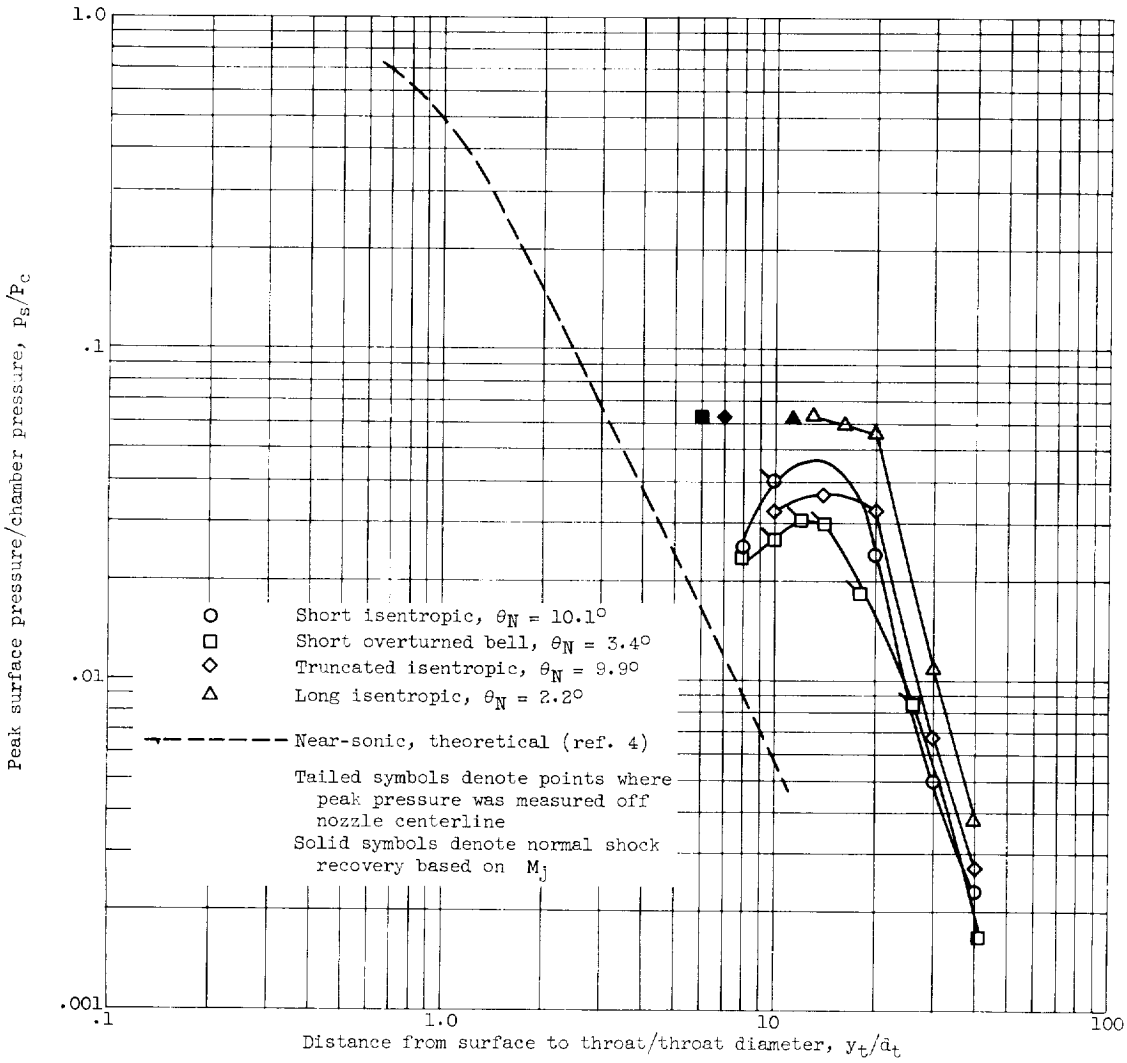

Figure 9. - Effect of nozzle contour on peak surface pressure.

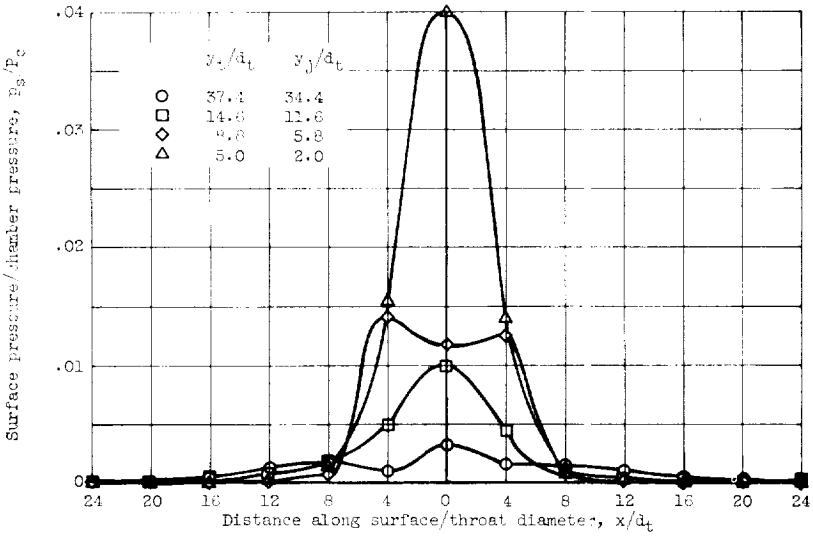

Figure 10. - Effect of clustering nozzles on landing surface pressure distribution. Short overturned bell nozzles; $\theta_N = 3.4^\circ$; $A_j/A_t = 25$; $l/d_t = 6.0$; $p_j/p_a = 545$.

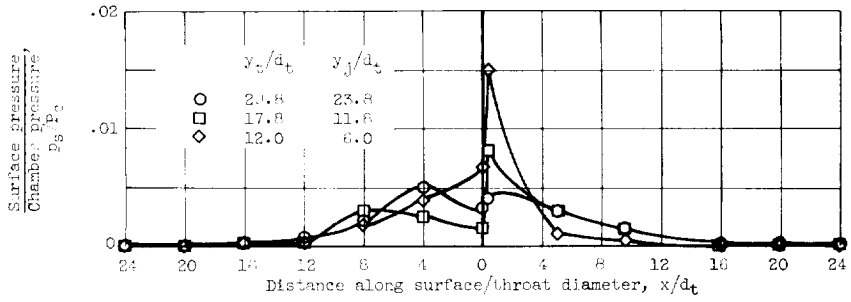

Figure 11. - Effect of a surface discontinuity on landing surface pressure distribution. Short overturned bell nozzle; $\theta_N = 3.4^\circ$; $A_j/A_t = 25$; $l/d_t = 6.0$; $p_j/p_a = 545$.

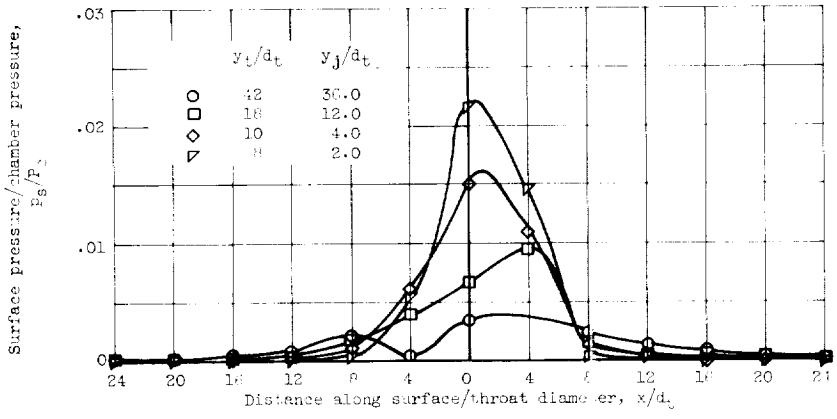

Figure 12. - Effect of operation at 5° inclination from vertical on landing surface pressure distribution. Short overturned bell nozzle; $\theta_N = 3.4°$; $\alpha = 5°$; $A_j/A_t = 25$; $l/d_t = 8.0$; $p_j/p_a = 545$.

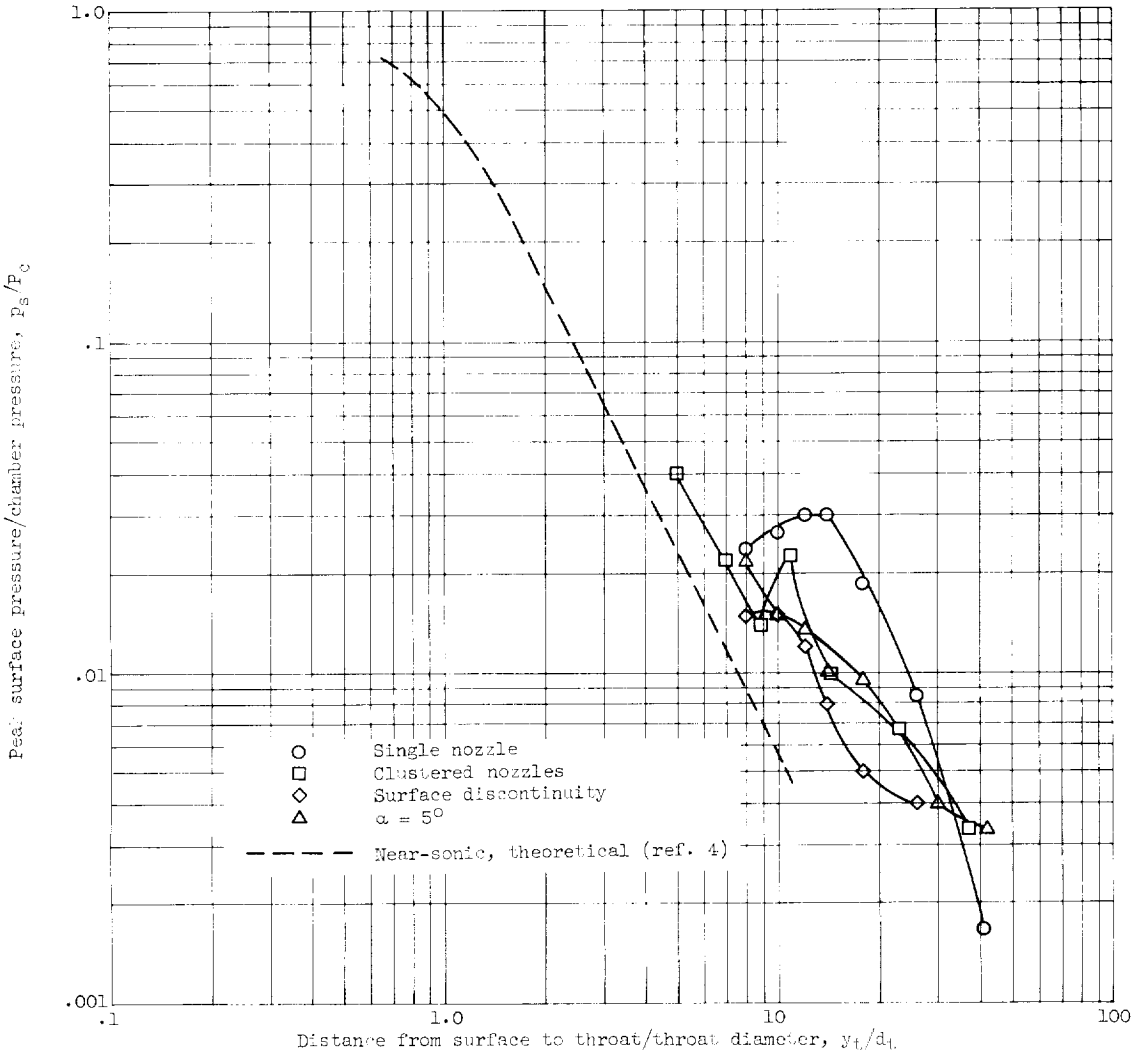

Figure 13. - Effect of clustering nozzles and approach conditions on peak surface pressure.

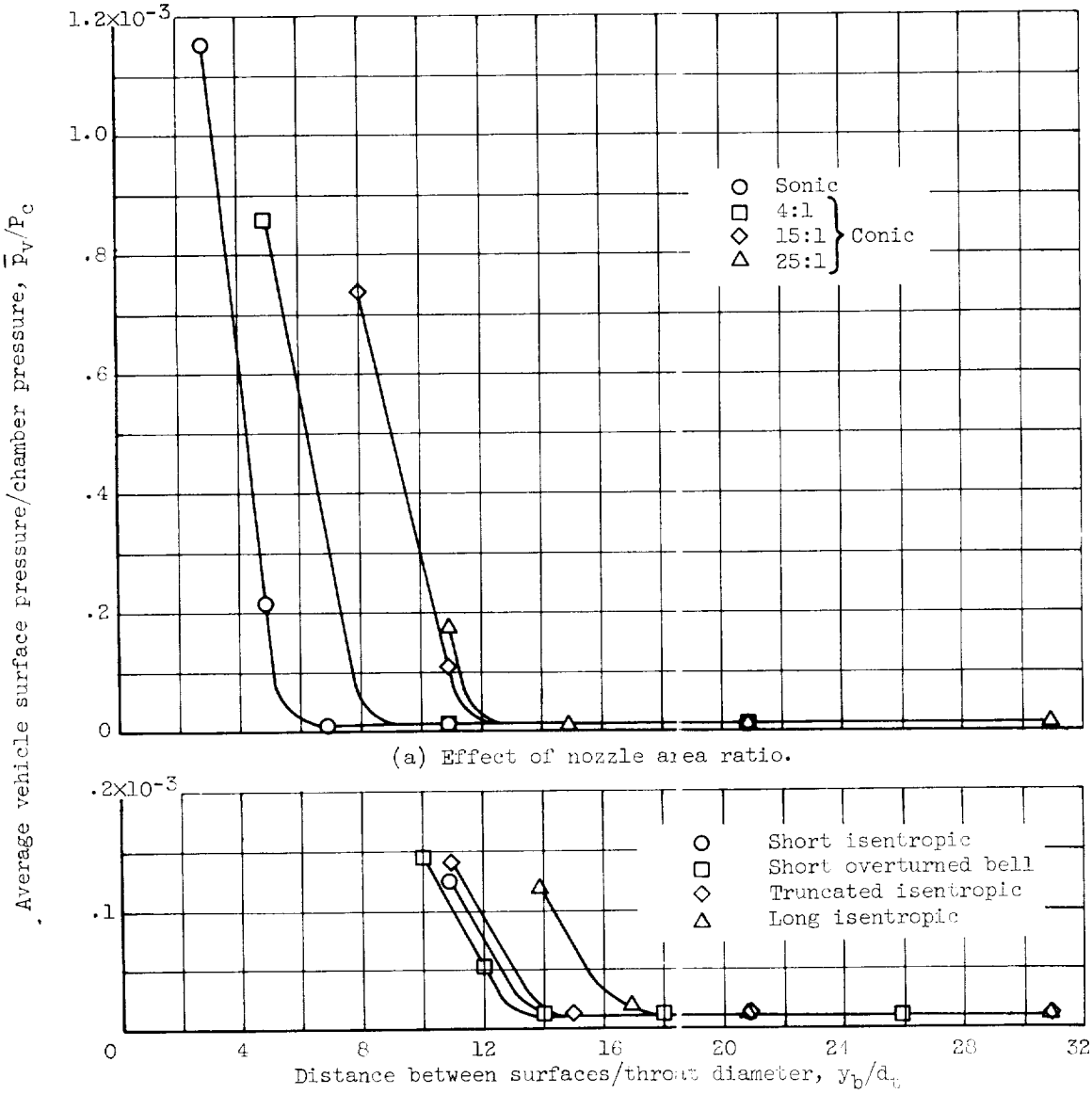

(a) Effect of nozzle area ratio.

(b) Effect of nozzle contour.

Figure 14. - Average pressure on cylinder face at various descent heights.

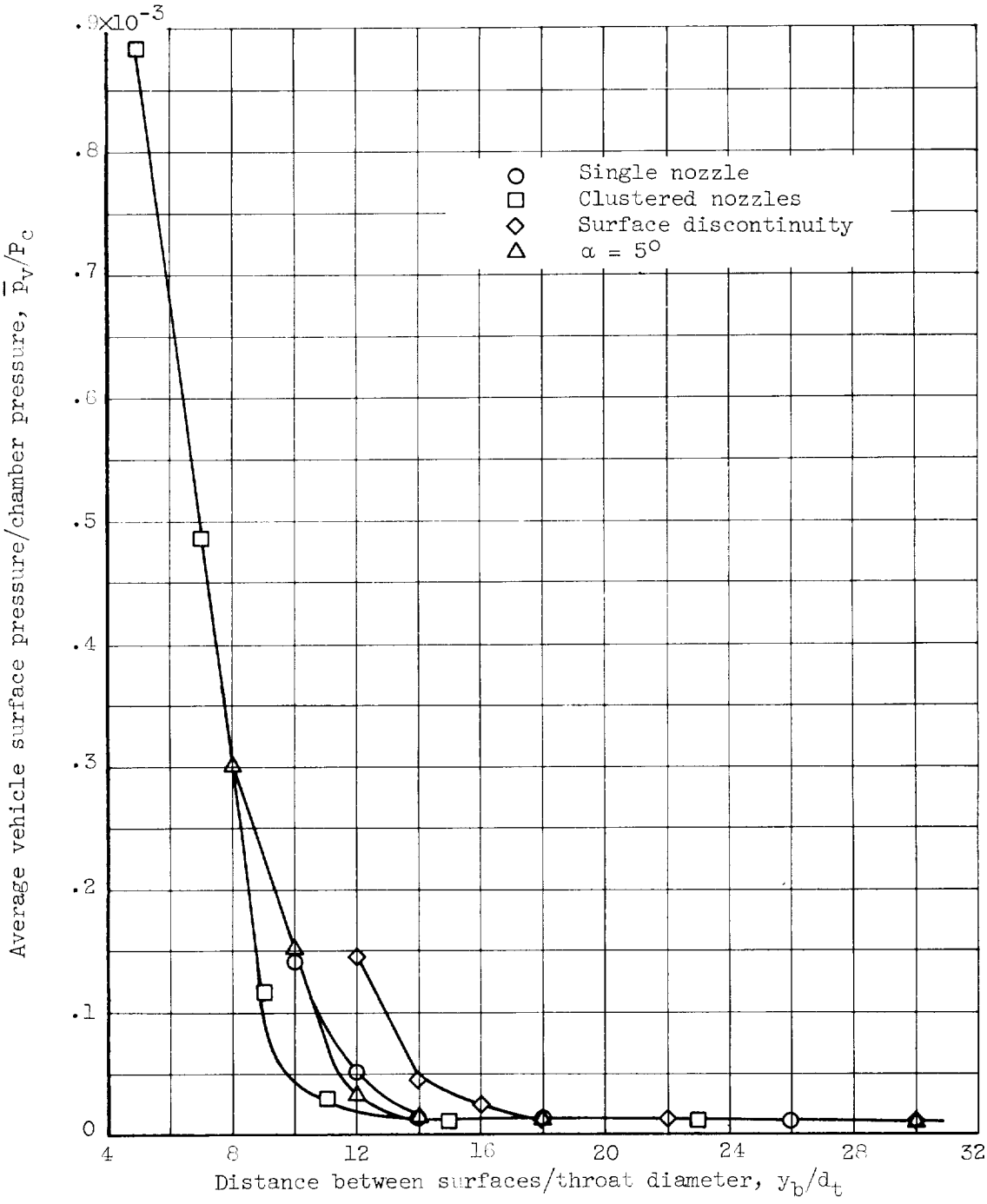

(c) Effect of clustering nozzles and approach conditions.

Figure 14. - Concluded. Average pressure on cylinder face at various descent heights.

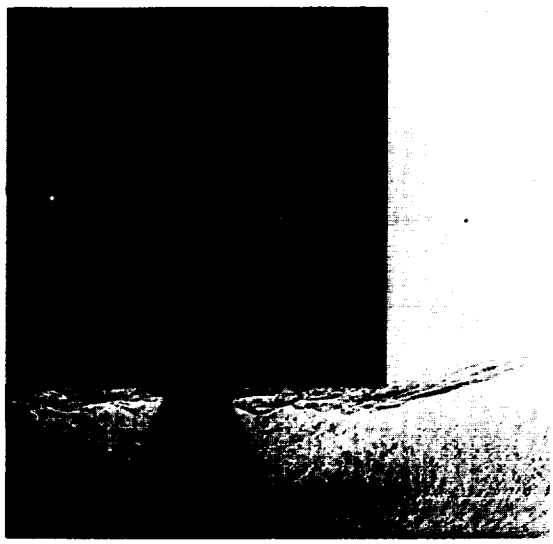

(a) Single nozzle. y_b/d_t = 10.

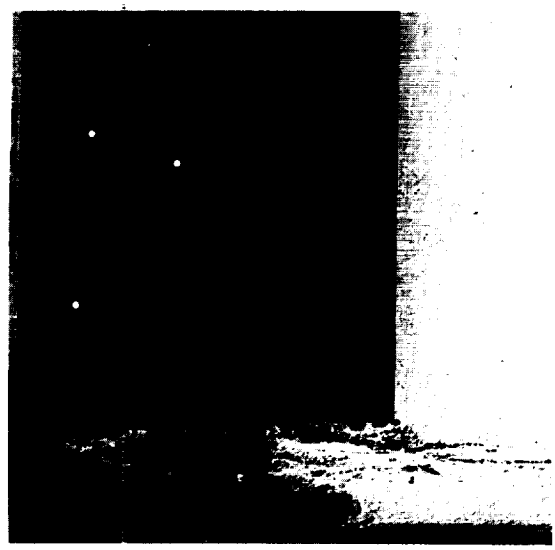

(b) Clustered nozzles. y_b/d_t = 7.0.

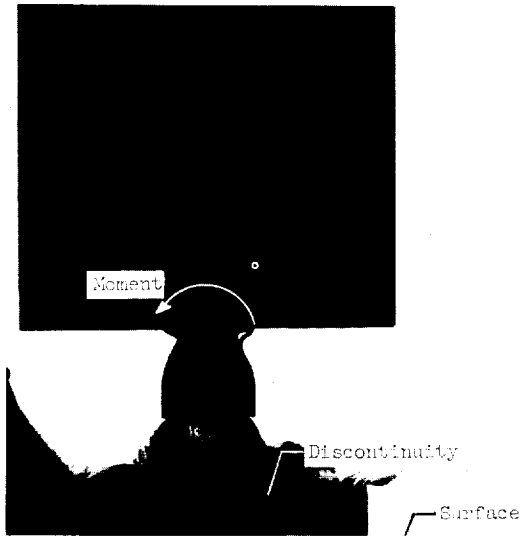

(c) Single nozzle with discontinuity. y_b/d_t = 14.

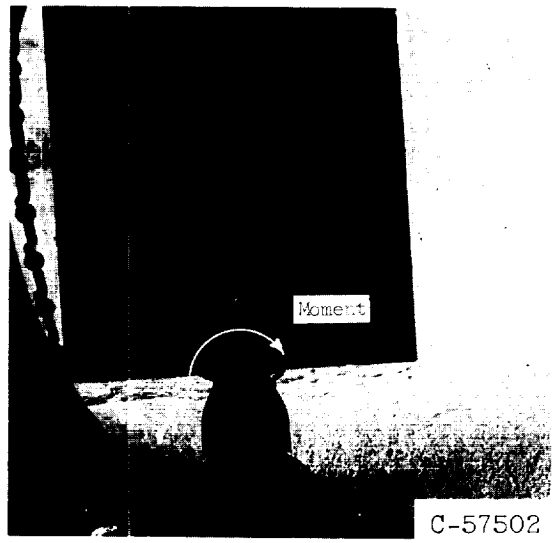

(d) Single nozzle at 5° inclination from vertical. y_b/d_t = 10.

Figure 15. - Reflected shocks on cylinder at close proximity to landing surface.

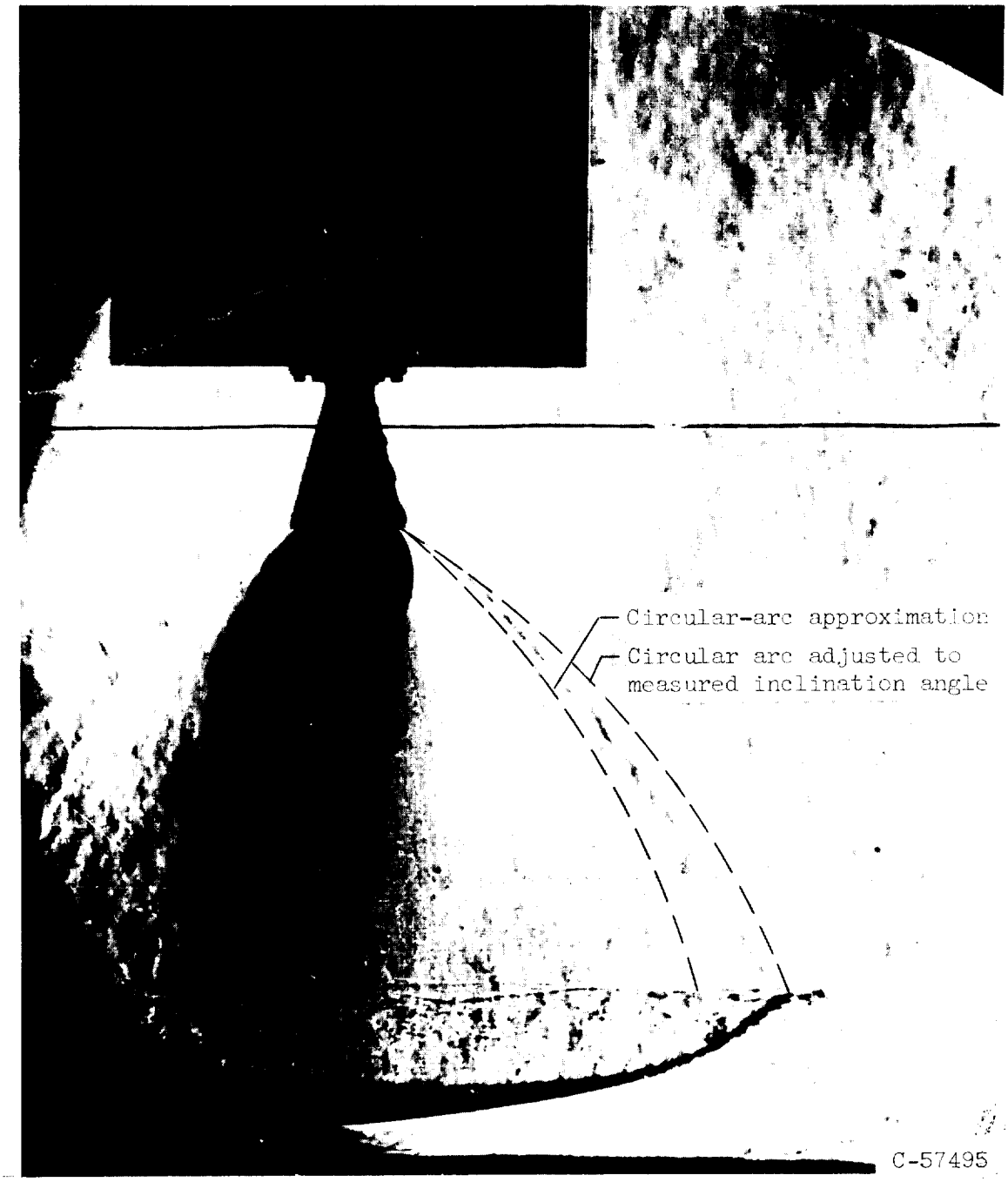

(a) Conical. $\theta_N = 15^\circ$.

Figure 16. - Comparison of theoretical and experimental jet boundaries. $A_j/A_t = 25$.

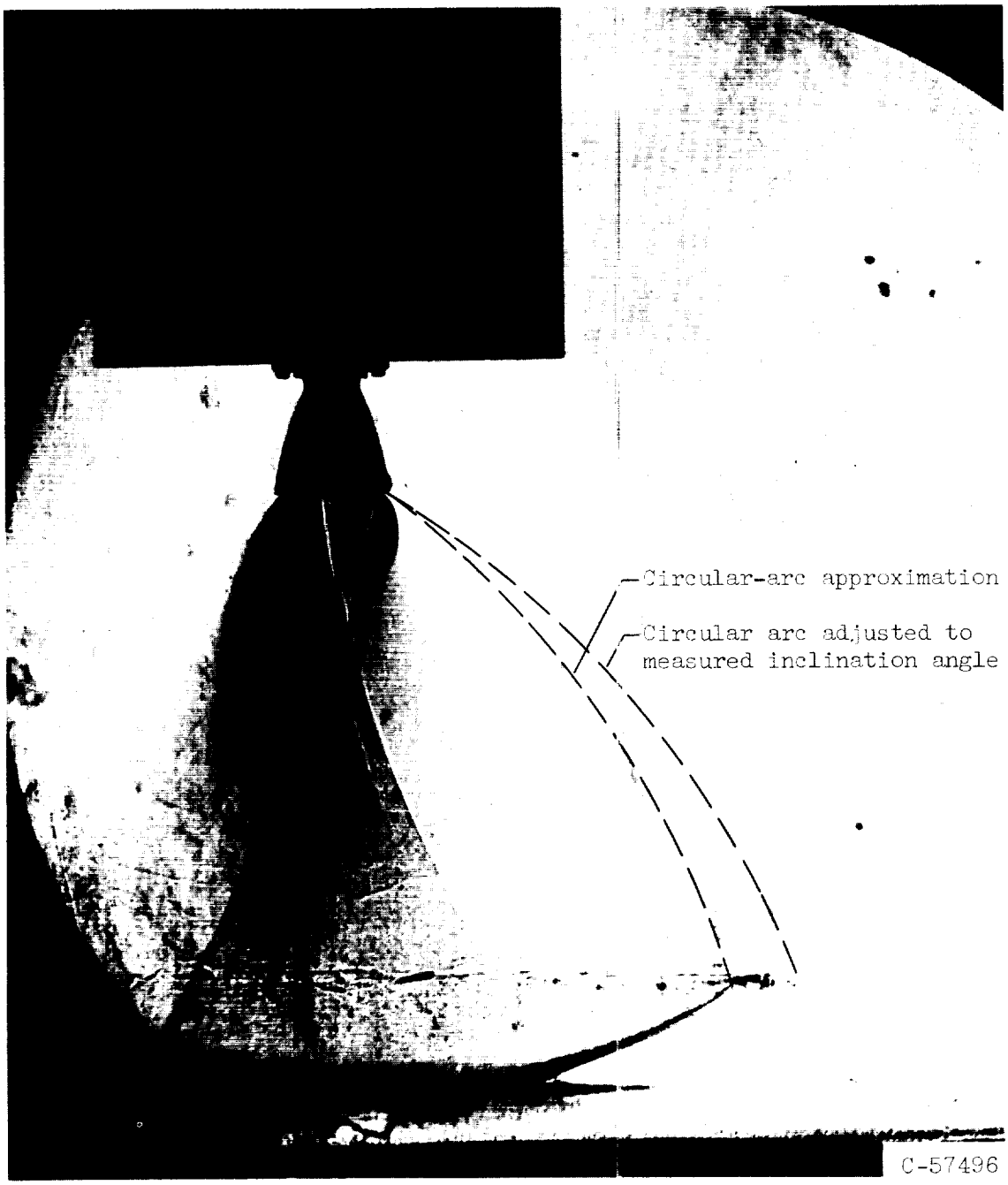

(b) Short isentropic. $\theta_l = 10.1^\circ$.

Figure 16. - Continued. Comparison of theoretical and experimental jet boundaries. $A_j/A_t = 25$.

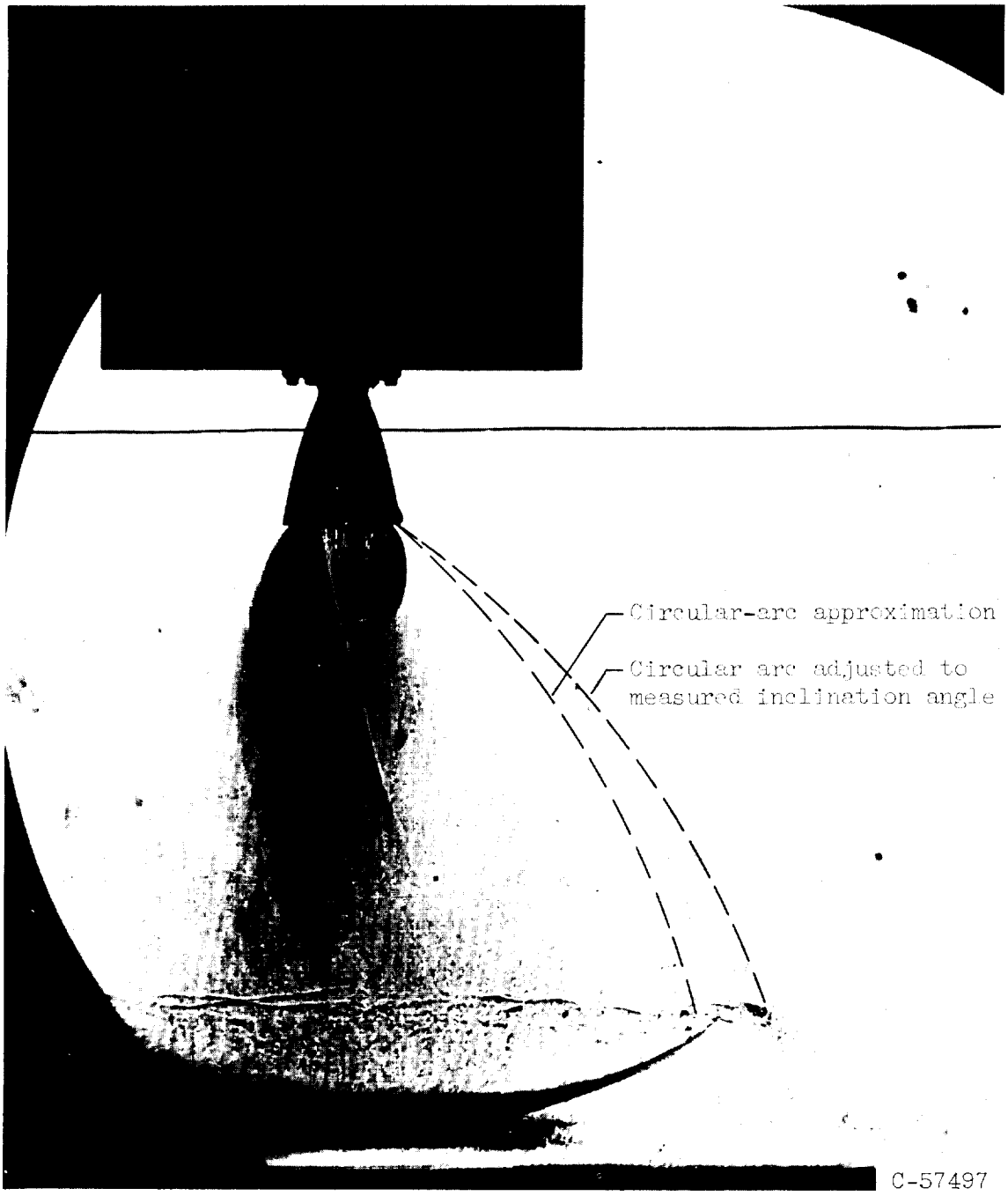

(c) Truncated isentropic. $\theta_N = 9.9^\circ$.

Figure 16. - Continued. Comparison of theoretical and experimental jet boundaries. $A_j/A_t = 25$.

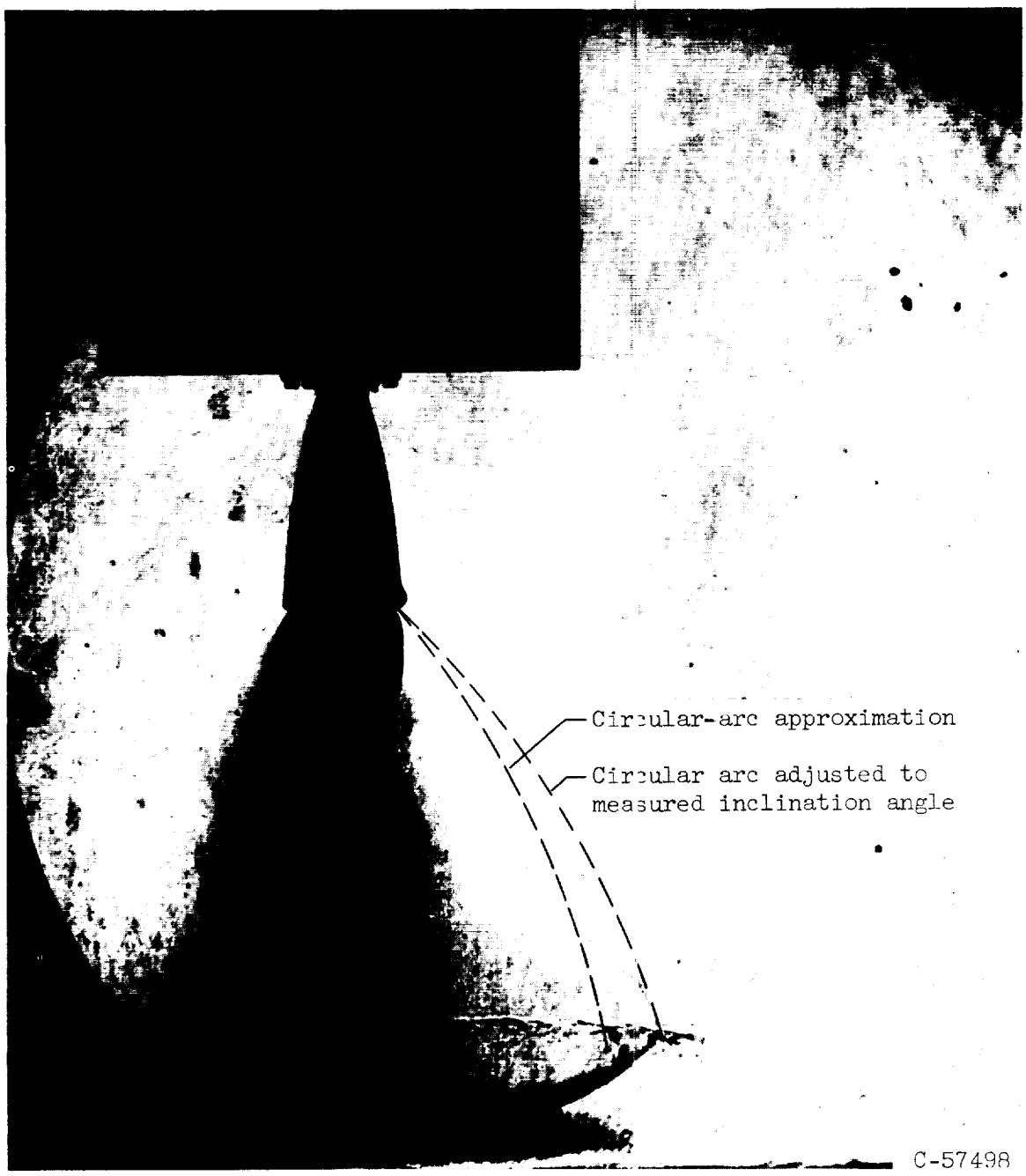

(d) Long isentropic. $\theta_N = 2.2^\circ$.

Figure 16. - Concluded. Comparison of theoretical and experimental jet boundaries. $A_j/A_t = 25$.

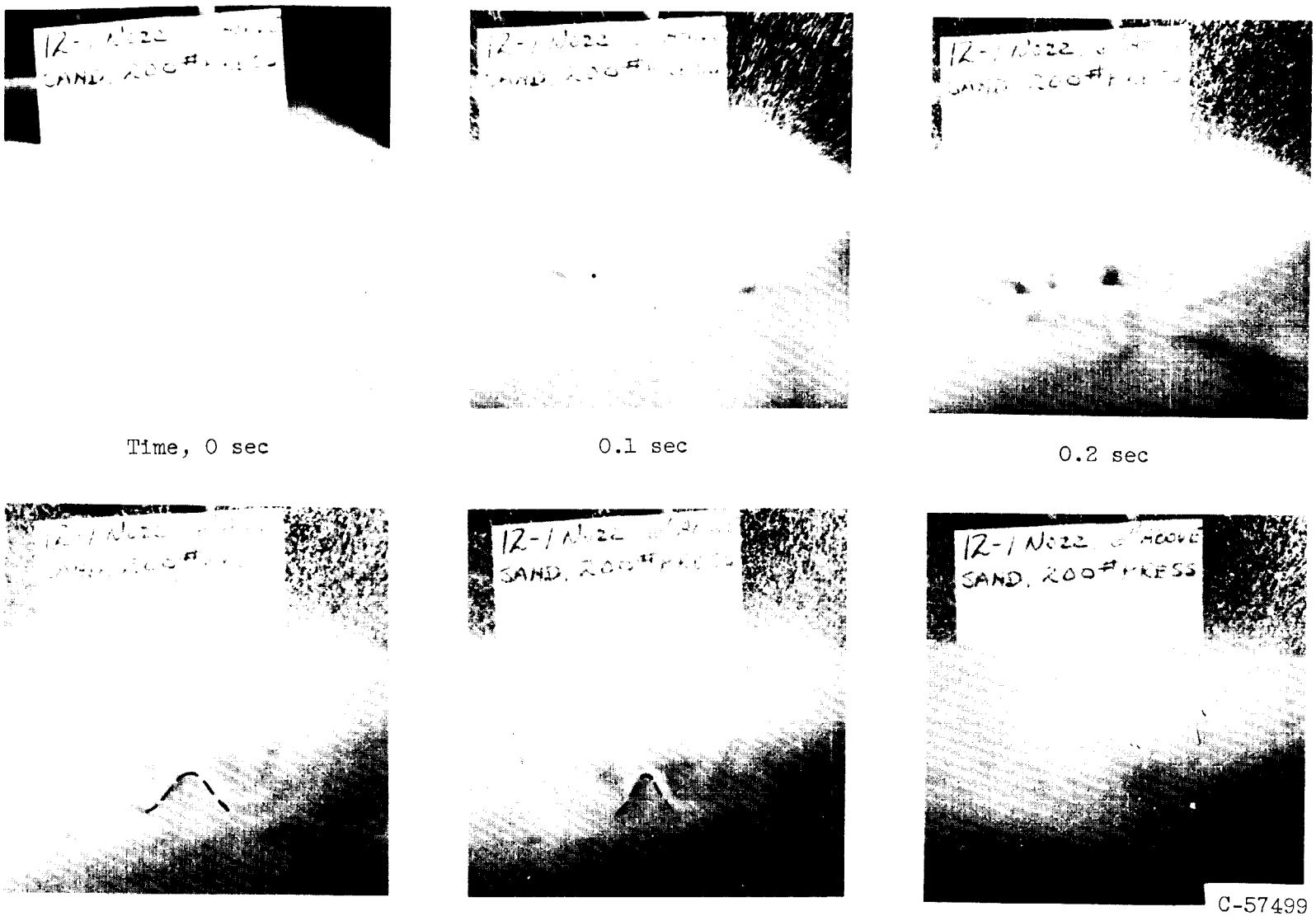

Figure 17. - Initial erosion pattern obtained at a descent height of 192 throat diameters.

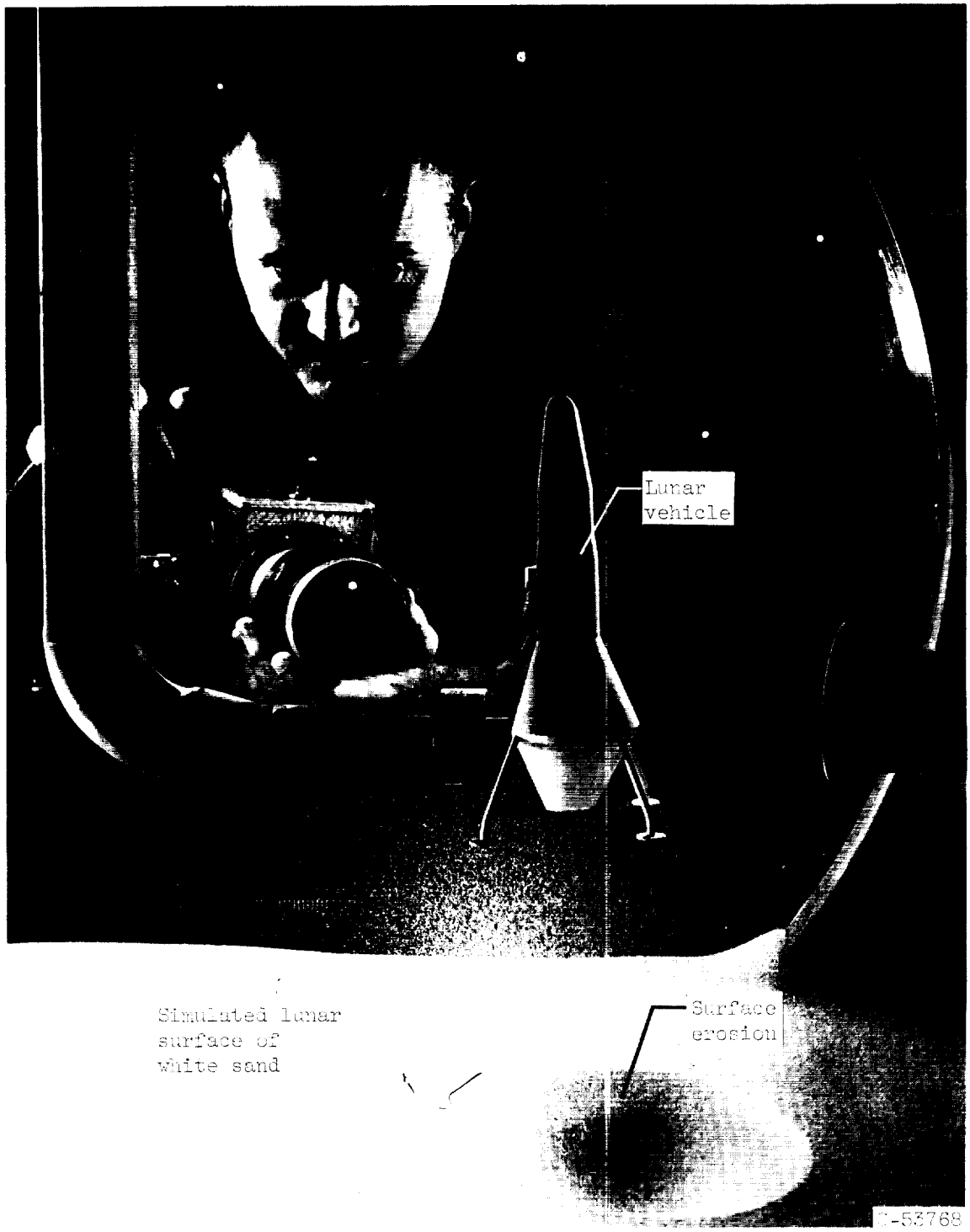

Figure 18. - Surface erosion in sand caused by an underexpanded jet of air.